THESIS

SELECTIVE REMOVAL OF FLUORINATED TIN OXIDE (SnO_2:F) FROM PILKINGTON TEC GLASS

Submitted by

Mathew Rekow

Department of Mechanical Engineering

In partial fulfillment of the requirements

For the Degree of Master of Science

Colorado State University

Fort Collins, Colorado

Fall 2017

Master's Committee:

Advisor: Walajabad Sampath

Don Radford
James Sites

ABSTRACT

SELECTIVE REMOVAL OF FLUORINATED TIN OXIDE (SnO2:F) FROM PILKINGTON TEC GLASS

High power lasers are utilized in a variety of processes in solar energy production and energy storage. In the production of CdTe (Cadmium Telluride) solar cells, pulse lasers are used for the so called P1 scribe step that is the first step in process of creating discrete series connected cells on an otherwise monolithic glass panel. A standard laser process sequence is well established in the industry. The common P1 process step removes all previously deposited materials, resulting in exposure of the soda lime glass substrate along the scribe line. These previously deposited layers include three layers deposited during the fabrication of the glass panel, an intrinsic SnO_2 layer, a SiO_2 layer, and the conductive SnO_2:F layer, the latter of which forms the transparent conductive front contact of the solar cell. If the CdTe film is applied immediately afterward, sodium diffuses from the glass into the deposited CdTe film and is detrimental to the performance of the CdTe solar cell (1). To mitigate this problem, commercial processes perform the P1 scribe after CdTe deposition and the resulting groove is filled with a photo-resist. This photo-resist application process accounts for a significant fraction of the capital equipment cost in a CdTe solar panel production line (2). A means of creating a Na barrier layer in situ would eliminate the requirement of the photo-resist application step and simplify the production process. This work is aimed at developing a laser based scribe process that removes the SnO_2:F layer but preserves the intrinsic SnO_2 layer and the SiO_2 layer to serve as a barrier to Na diffusion and hence eliminate the need for the photoresist application step. During this work, a very unusual laser-material interaction was discovered where the laser appears to initiate a physical – chemical reaction that proceeds along an unusual and apparently undescribed pathway that has many of the characteristics of an etch process. This laser “etching” mechanism allows arbitrary reduction of the film thickness in a controlled manner on the scale of a few microns. In addition to the fine depth selection, we find that there develops a laser pulse duration dependent microstructure on the surface. The unusual characteristics of this interaction are examined, and a physical model is proposed to describe it. Finally, sodium diffusion effects were measured, and other potential applications of this novel process are explored.

ACKNOWLEDGMENTS

This work was performed as a collaboration between Colorado State University, ESI-PyroPhotonics Lasers Inc and Abound Solar in 2011. The work was primarily motivated by the desire of my employer at the time (ESI Inc.) to find new applications in the solar industry for a new type of fiber laser. At the time, my position was director of the ESI-PyroPhotonics laser applications laboratory and by coincidence I was simultaneously engaged in pursuit of a Master of Science Degree in Materials Engineering through the distance program at Colorado State University, taking several courses under Doctor Sampath, a founder of Abound Solar. The laser work was performed in the ESI laser applications lab in Fremont, California. Deposition of active layers was performed at NSF I/UCRC for Next Generation Photovoltaics at CSU, with test evaluation performed by Abound Solar. In addition, some EDX work was performed at NRC Canada, Industrial Materials Institute, a contractor to ESI.

Unfortunately, changing economic conditions in the solar industry effectively removed the driving forces behind this work. This combined with initial panel test results that were not encouraging combined stop further process development work. Even so it is my hope that this work will find application in future energy and electronics applications as transparent conductive oxides are a fundamental material both for energy production, display and microelectronics. I would like to thank and recognize the following individuals for their contribution and support of this work.

NSF I/UCRC for Next Generation Photovoltaics, Colorado State University, Fort Collins, CO, USA

- Doctor W. S. Sampath
- Paul Kobyakov – Graduate Student

ESI-PyroPhotonics (Eolite) Lasers, Inc. 275 Rue Kesmark, Dollard-des-Ormeaux, Québec H9B 3J1, Canada

- Doctor Tullio Panarello
- Doctor Richard Murison

Abound Solar

- Scott Jensen
- Anders Olsson

NRC Canada, Industrial Materials Institute-CAMM, 800 Collip Circle, London, Ontario NG6 4X8 Canada

- Doctor Suwas Nikumb
- Craig Dinkel

TABLE OF CONTENTS

1.0 BACKGROUND AND SIGNIFICANCE

1.1 BACKGROUND

Fluorinated SnO_2 is one of the most common transparent conductive oxide (TCO) materials in use to today. Under the Pilkington brand name, it is typically referred to as TEC series glass. Its primary use is in architecture glass as a heat reflector due to its low emissivity (Low-E) characteristics. Another large application is as an inexpensive substrate for CdTe solar cells. This and related materials are utilized for other energy production technologies such as direct solar water catalysis, flat panel display and microelectronics. This SnO_2:F film is typically deposited on soda lime glass in a layer from a few hundred Å to 1µm in thickness depending on the application. To make a device based on these TCO films, typically the film must be patterned by some means. For example, in the case of CdTe solar cells, the film is removed in periodic thin strips along the length of the substrate to create a series of electrically isolated pads. Likewise, other applications generally require patterning of electrically isolated structures. This work is specifically aimed at developing a novel process of patterning TEC10 glass substrates with a pulse laser source for the production of CdTe solar cells.

1.2 TEC 10 GLASS STRUCTURE

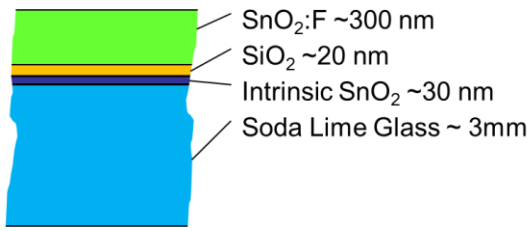

FIGURE 1: CROSS SECTION DEPICTING THE STRUCTURE OF TEC 10 GLASS FROM PILKINGTON.

1.3 STRUCTURE OF THIN FILM SOLAR CELLS

Thin film solar panels are not a recent innovation. The first commercial thin film solar panels were based on amorphous silicon films grown on glass, becoming commercially available in the 1970s. The process of producing a thin film solar cell involves deposition of a conductor, semiconductors to form a P-N junction and finally another conductor on a suitable substrate. This thesis will not go into detail regarding the physics of photovoltaic cells, but of key importance to the operation of the final panel is the output voltage and current characteristic. For a single cell, the voltage generated is a function of the band gap of the semiconductor materials system involved. For example, a single CdTe photovoltaic cell produces about 0.8 Volt (3) and a maximum current dependent upon the total area of the cell. This presents an obvious problem for scaling up thin film solar panels for commercial power production. First, a large single solar cell of with a few square meters of surface area would produce an impractically large amount of current at a very low voltage. Higher voltages and lower currents are preferred for efficient power transmission purposes. The industry solved this problem in amorphous silicon by developing what has come to be commonly known as the P1, P2, and P3 process steps. A fourth operation, often referred to as P4, removes shunts at the edges and prepares the module for electrical interconnect and encapsulation. Figure 2(A-F) shows a generic sequence of laser process steps that create a monolithically interconnected structure like those used in fabrication of amorphous silicon or CIGS (Copper Indium Gallium Selenide) solar cell module. Figure 2G illustrates the physical and electrical structure of a processed module consisting of three cells electrically connected in series.

Referring to Figure 1, the process steps are as follows:

A) A bottom conductive layer is applied to a substrate.

B) P1 Process Step: A pulse laser beam is utilized to remove the conductive layer completely in stripes across the substrate to generate electrically isolated pads.

C) The active semiconductor layers are deposited over the newly formed pads to form a P-N junction.

D) P2 Process Step: A pulse laser beam is utilized to remove the active semiconductor material terminating on the bottom conductive layer slightly offset from the P1 scribe. This forms a via trench through the semiconductor to the conductive layer below.

E) A top transparent conductive layer is applied that is conformal to the laser cut via trenches.

F) P3 Process Step: Again, a pulse laser beam is utilized to remove the top conductive layer along a trench that terminates on either the bottom conductive layer or alternatively on the semiconductor layer and that is slightly offset from the P2 scribe and the P1 scribe.

G) P4 Process Step: Finally, laser or other means is utilized to remove material from the edges of the substrate to prepare the substrate for electrical contacting and encapsulation. Figure 1G depicts the completed and functional solar panel consisting of three series interconnected cells.

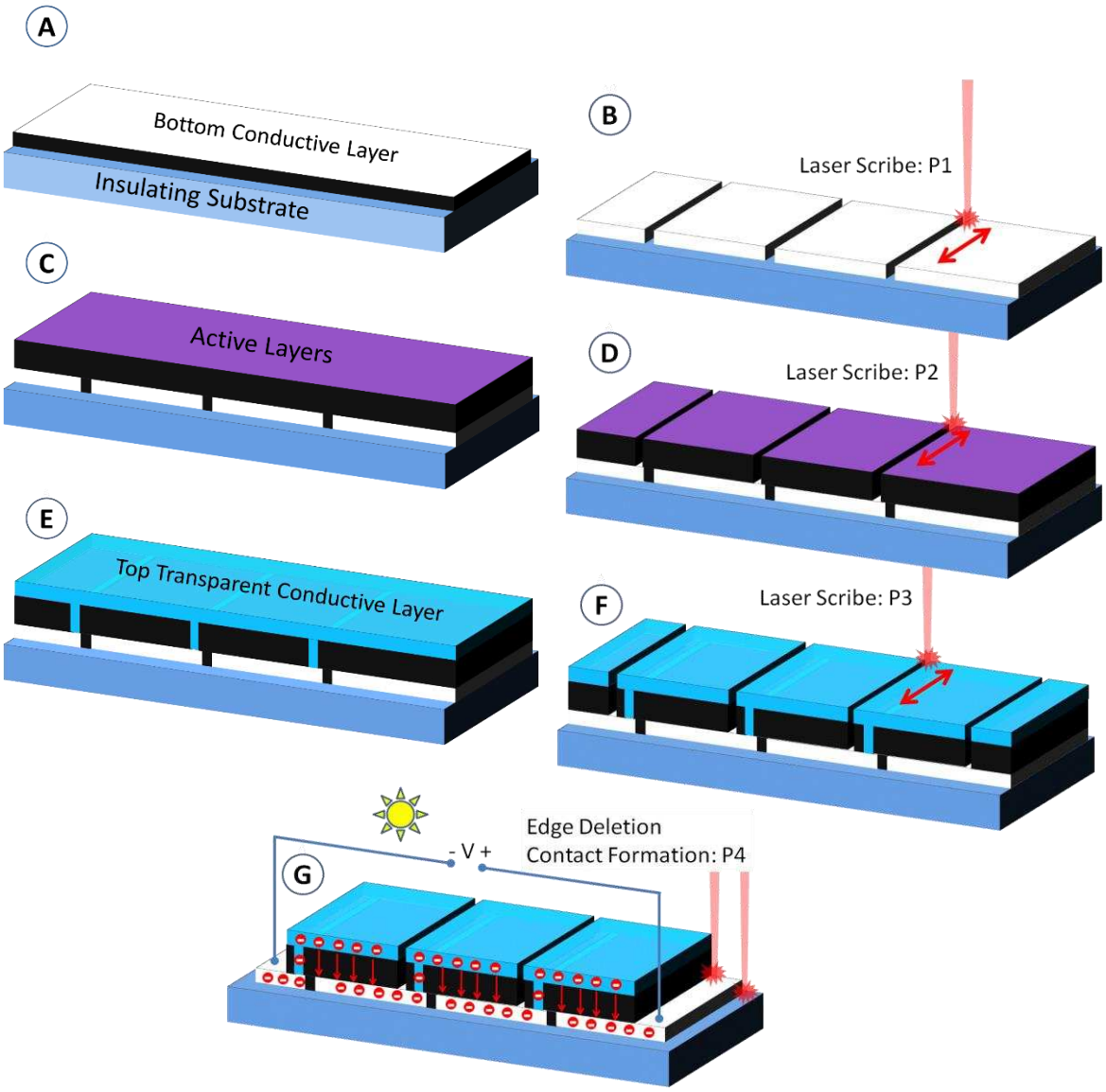

FIGURE 2: SEQUENCE OF LASER PROCESSING STEPS REQUIRED TO FABRICATE MONOLITHIC SERIES INTERCONNECTS FOR AN AMORPHOUS SILICON OR CIGS MATERIAL SYSTEM.

CdTe solar panels also utilize a set of analogous laser processes applied in a slightly different manner. The primary difference is that for CdTe solar cells, bottom layer is the transparent conductive layer applied to the glass substrate, the top layer is generally an opaque conductive material and solar flux impinges upon the solar cell from the bottom of the substrate rather than from the top. Otherwise the structures are analogous to those shown in Figure 2. However due to the phenomenon of Na diffusion and its negative impact on performance and lifetime of

CdTe solar cells the laser processing steps are modified as shown in Figure 3 by modifying the sequence of steps and filling the P1 scribe with a photoresist.

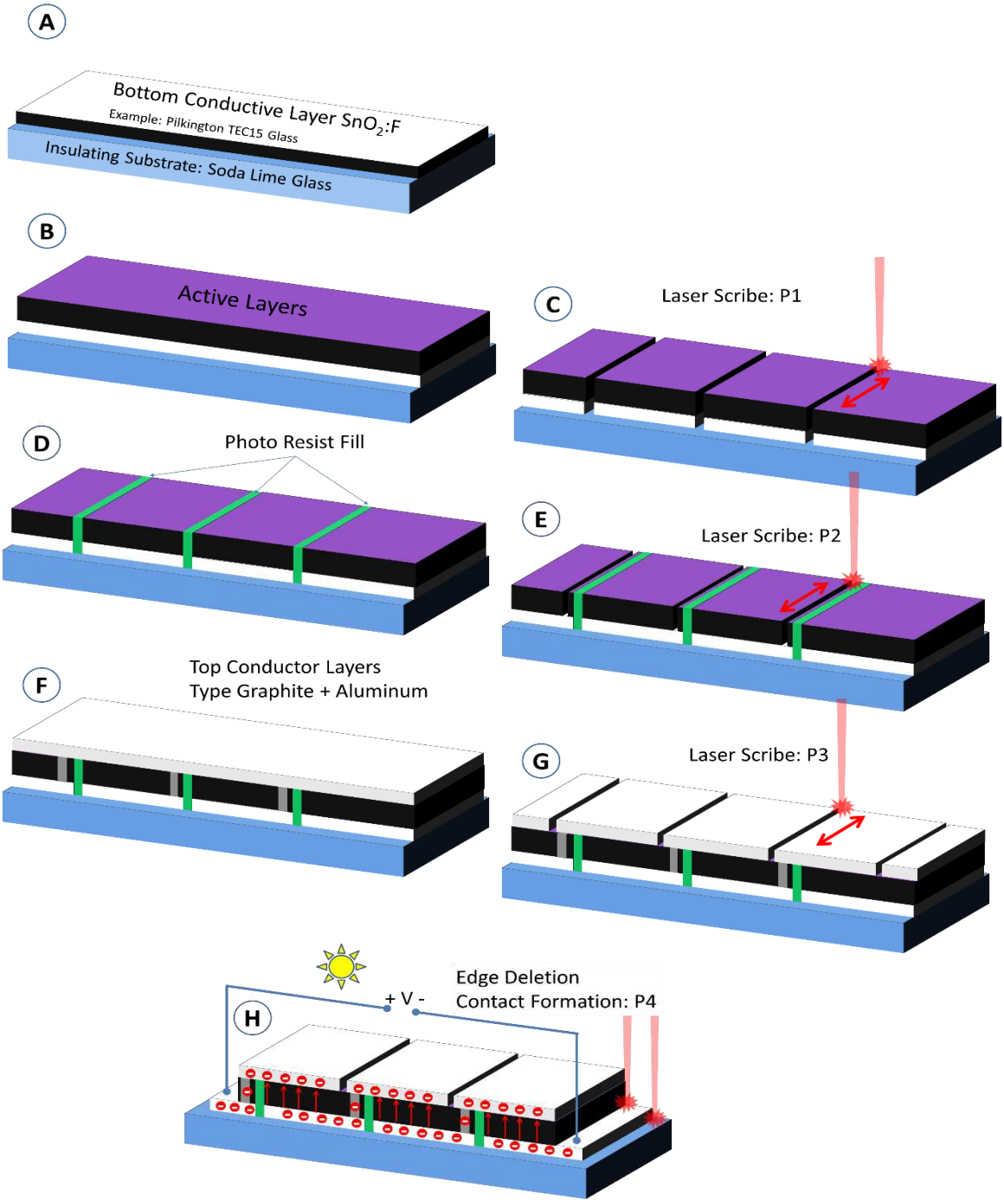

FIGURE 3: SEQUENCE OF LASER PROCESSING STEPS REQUIRED TO FABRICATE MONOLITHIC SERIES INTERCONNECTS FOR AN CDTE MATERIAL SYSTEM.

Referring to Figure 3, the process steps are as follows:

A) A bottom conductive layer is applied to a soda lime glass substrate, typically during glass fabrication.

B) Active CdTe semiconductor layers are deposited.

C) P1 Process Step: A pulse laser beam is utilized to remove the active material and the conductive layer completely in stripes across the substrate to generate electrically isolated pads.

D) The P1 scribe grooves are backfilled with a photoresist and the excess is removed leaving only the photoresist in the grooves.

E) P2 Process Step: A pulse laser beam is utilized to remove the active semiconductor material terminating on the bottom conductive layer slightly offset from the P1 scribe. This forms a via trench through the semiconductor.

F) A top conductive layer is applied (typically graphite) that fills the laser cut trenches and an aluminum back contact layer is applied.

G) P3 Process Step: Again, a pulse laser beam is utilized to remove the top conductive layers along a trench that terminates on either the bottom conductive layer or alternatively on the semiconductor layer and that is slightly offset from the P2 scribe and the P1 scribe.

H) P4 Process Step: Finally, laser or other means is utilized to remove material from the edges of the substrate to prepare the substrate for electrical contacting and encapsulation. Figure 3-H depicts the completed and functional solar panel consisting of three series interconnected cells.

In comparing the two processes, the photoresist fill adds and extra step. This additional step also tends to be a particularly messy and time-consuming step. Additional process steps required by the photoresist step are mixing, application, drying, curing, and cleaning to name a few. A significant portion of the waste stream from a CdTe solar panel factory is related to this process step. It is estimated that 20% of the capital expenditure for a CdTe process line is related to this process step (2), clearly there is a strong economic incentive to eliminate this photoresist process step. Figure 4 shows a completed real solar panel with the P1, P2 and P3 scribes clearly visible.

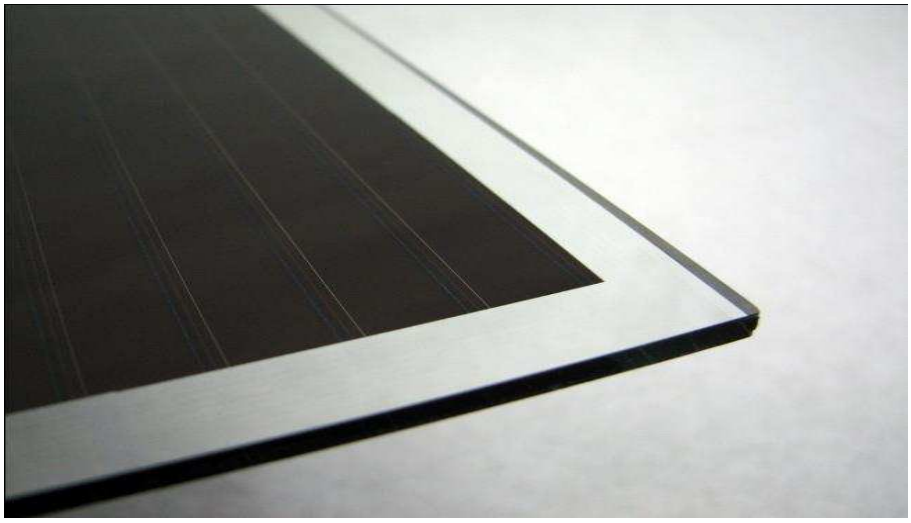

FIGURE 4: EXAMPLE OF A REAL THIN FILM SOLAR PANEL SHOWING THE P1, P2 AND P3 SCRIBES THAT FORM THE SERIES INTERCONNECT.

1.4 SODIUM DIFFUSION AND THE CDTE P1 SCRIBE

Before continuing it is necessary to discuss why filling the P1 scribe with photoresist is necessary in the first place. Figure 5 describes a hypothetical process in CdTe where the P1 scribe is applied prior the active layer material deposition in a manner similar to CIGS and amorphous silicon. In the first step at the left of Figure 5, the laser is used to remove the TCO layers that were deposited during Tec 10 glass manufacture. The middle illustration depicts the deposition of CdTe over the P1 scribe and the right illustration depicts the resultant diffusion of sodium ions from the soda lime glass substrate into the CdTe layer. The diffusion of Na ions into the CdTe layers causes rapid degradation of the cell performance and causes cell failure in a matter of hours (1). For contrast, Figure 6 depicts the process steps commonly utilized in industry to create a sodium diffusion barrier after the fact. While the physical mechanism behind this degradation is outside the scope of this thesis, there are numerous references in the literature and private communications with personnel from two different CdTe solar panel manufacturers confirmed the severity of the problem and the need for the photoresist step to mitigate the problem. Furthermore, soda lime glass contains about 15% sodium oxide so it is clear that there is a very large reservoir of sodium and a large concentration gradient to drive diffusion (4).

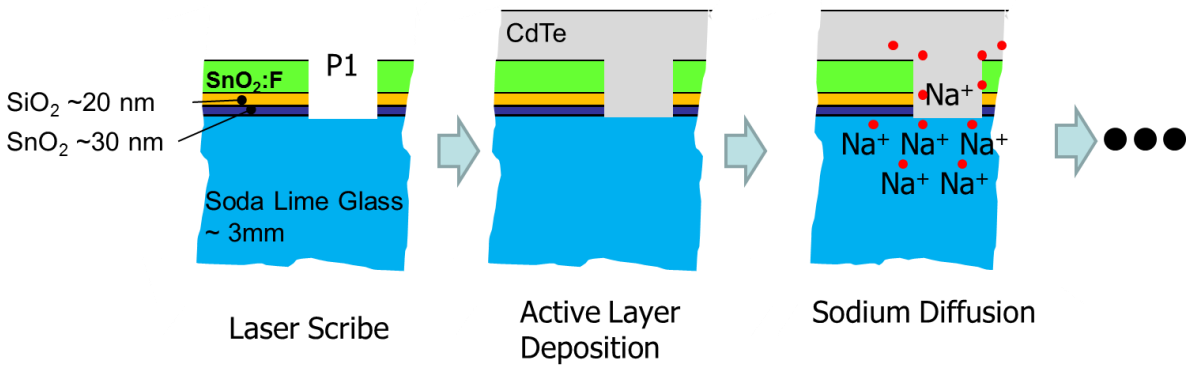

FIGURE 5: EXAMPLE OF RESULTING SODIUM DIFFUSION THAT WOULD OCCUR IF THE P1 LASER SCRIBE WAS APPLIED PRIOR TO CDTE DEPOSITION.

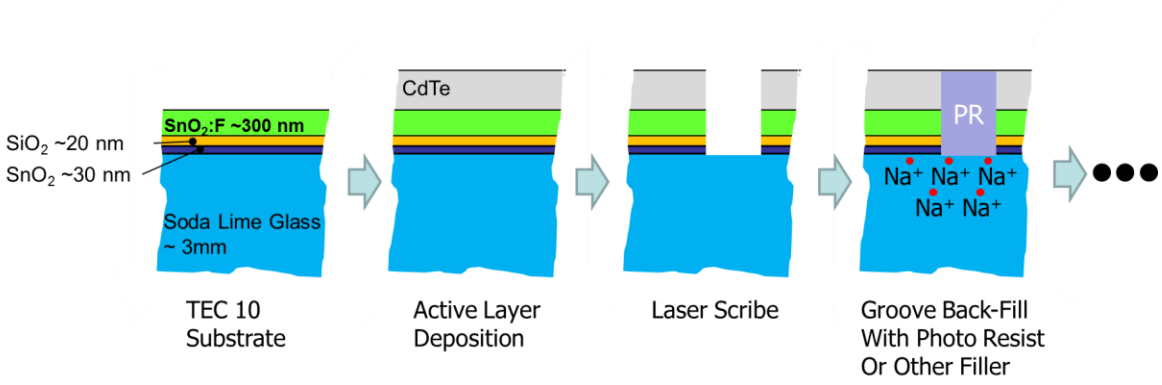

FIGURE 6: GENERIC PROCESS USED IN INDUSTRY TO FORM THE P1 ISOLATION SCRIBE FOR CDTE SOLAR CELLS AND TO PRODUCE A BARRIER LAYER AFTER THE P1 LASER SCRIBE IF APPLIED.

1.5 AIMS

This work was originally aimed at demonstrating a novel way to perform the P1 scribe for CdTe solar cells. The intent was that with depth selective laser ablation, the conductive layer could be removed while preserving an underlying insulating SiO_2 and intrinsic SnO_2 layers, as a barrier to Na diffusion from the glass. Figure 7 below illustrates this ideal CdTe P1 scribe process and resultant solar cell structure that would result by preservation of the SiO_2 and SnO_2 layers. This structure if viable could eliminate the need for the photoresist application step.

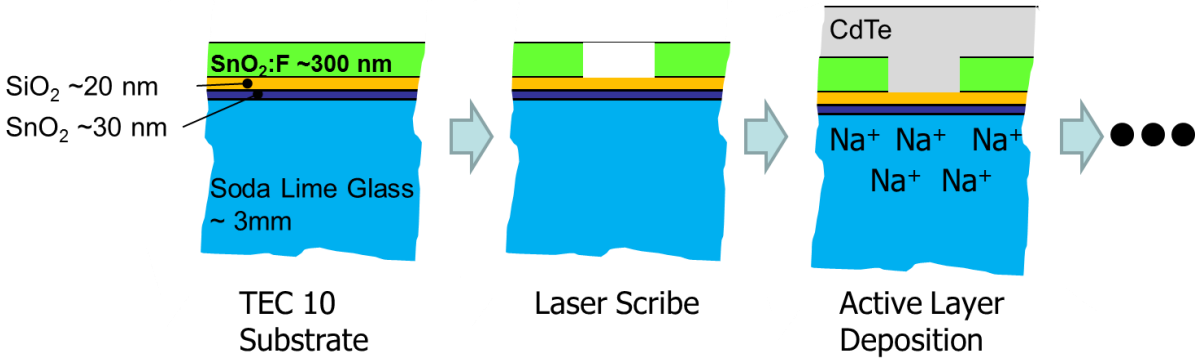

FIGURE 7: IDEALIZED CDTE SOLAR CELL STRUCTURE UTILIZING A NEW LASER PROCESS FOR THE P1 LASER SCRIBE THAT PRESERVES THE BARRIER LAYERS INTACT.

As this thesis will show, the SiO_2 and SnO_2 layers were preserved, but subsequent tests appeared to indicate that the rates of Na diffusion remained unacceptably high. There were some questions regarding the validity of the test protocol however the initial negative test result combined with changes in the solar business climate combined to reduce the interest in this process development both on the part of Abound solar and my own employer ESI. The aim of this research then shifted to understanding this novel ablation mechanism and proposing other potential applications.

1.6 SCIENTIFIC MERIT AND APPLICATIONS

While the applicability of this process to produce CdTe solar panels was not conclusively proven or disproven, the discovery of this novel material removal mechanism opens the possibility to other new applications. Examples could include direct writing of holographic images, writing passive electronic components, and creating structures for active transparent electronic devices and the like (5). In addition to thickness reduction the discovery of a pulse duration and polarization dependent microstructure that results in a strong diffraction effect also has interesting applications. This microstructure imparts apparent color to the film surface that can be tuned by controlling the pulse duration. Finally, even in the present solar environment that is dominated by cheap crystalline and polycrystalline solar cells from China, one CdTe company, First Solar, has maintained its competitive market share

and position. It is possible that this work could help to reduce the cost of CdTe panels still more to help them maintain their competitive market position.

1.7 GAPS IN PREVIOUS KNOWLEDGE

There are two mechanisms of laser ablation with pulse lasers that are commonly encountered in laser processing of materials (6). The first mechanism generally consists of delivering so much energy into a volume of material that the atoms that make up the material become ionized. With the outer electrons stripped away the material lattice falls apart and repulsive electrostatic forces drive the remaining material away from the target surface. A second thermal mechanism induces a phase change from solid to liquid and then from liquid to gas. The expanding vapour then removes any remaining liquid material in an explosive manner. Both mechanisms have characteristic traits such as a ridge of recast material at the edge of an ablation pit as well as a pit topography that is reminiscent of the intensity profile of the beam (typically Gaussian). In this work on SnO_2:F we have observed an ablation pit morphology that is fundamentally different in character compared with these more well-known processes of ablation. Namely we find a pit profile with a flat bottom, no recast material, and a depth that depends only on the laser temporal pulse duration. Furthermore, there is no dependence on the laser spot energy profile or even the total energy contained within the pulse. These features imply that there is a third mechanism of laser material removal that is distinct from the better-known processes described above.

1.8 MATERIAL REMOVAL MECHANISM HYPOTHESIS

Our observations of this unusual ablation mechanism lead us to hypothesize that this laser material removal process is not laser ablation in the classical sense, but rather a laser induced physical material transformation. It was suggested that the laser could be driving sublimation of the TCO however factors such as the lack of dependency upon laser pulse energy do not support the concept of a phase transformation driven process. Namely, one would expect the process to proceed proportionally to the energy input. Data seems to support that there is a fundamental reaction rate that limits how quickly the process can proceed. Specifically, I hypothesize that the process is initiated by surface absorption and that decomposition from SnO_2:F to Sn_2+O_2+F plays the

primary role in driving this material removal process. The latter part of this thesis will consist of developing a physical model for this novel laser material removal mechanism and comparing the model against the observed physical process characteristics. If confirmed, this process represents an alternative means of processing these and other types of materials with “photo driven” thermo-chemical reaction compared to the more direct laser ablation mechanisms commonly utilized in industry. This type of process has certainly been studied and text books exist on utilization of lasers to drive chemical reactions, however utilization of laser driven chemistry to physically remove and structure materials does not appear to have been reported in laser materials processing literature. Most commonly, the laser is utilized to physically remove material, rather than to drive a chemical reaction that results in precise material removal. Hopefully this work may open the door to an alternative methodology that has not been previously well known.

2.0 MATERIALS AND METHODS

2.1 LASER SOURCE

For this work, we utilize the PyroFlex™-25 – 1064nm pulsed fiber laser from EOlite Systems Inc. This laser provides up to 25 Watt of average power. Unlike more traditional lasers, this fiber laser technology allows pulse durations to be varied from approximately 1 to several 100's of nanoseconds with 1 ns resolution. Furthermore, the laser system allows independent control of the pulse amplitude ns by ns which allows the construction of arbitrary temporal pulse shapes. These pulse shapes are achieved independent of laser repetition rate, which can be varied up to 500 kHz. Figure 8 below illustrates the difference between the PyroFlex laser and the typical "Q-switched" lasers that are used in the solar industry for the various laser scribe processes. The classic Q-switched laser is characterized by a rapidly rising leading edge followed by an exponentially decaying tail. This shape is a function of the laser cavity design and is for the most part a fixed feature of the laser. By contrast the PyroFlex laser system allows the production of arbitrary pulse energy distributions in time. As the figure shows the laser pulse can be generated to take on the "rectangular" shape, the "chair shape" or any other shape. As it turns out, many laser processes are very sensitive to the rate at which the laser energy is delivered. This temporal pulse shaping was key to developing and achieving the results in this thesis.

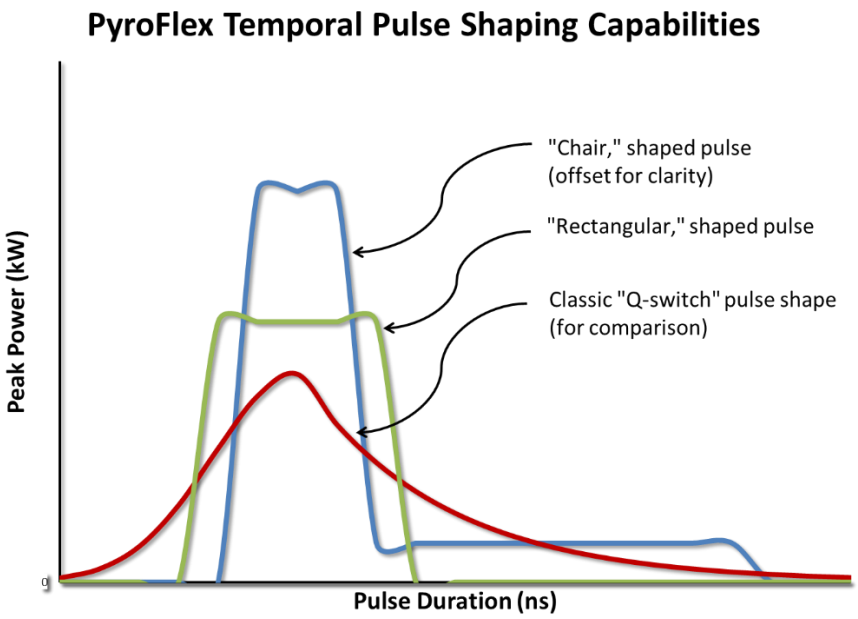

FIGURE 8: EXAMPLE OF PYROFLEX LASER TEMPORAL PULSE SHAPING CAPABILITIES.

2.2 OPTICAL SET UP

The 1064 nm laser beam was expanded and collimated to a diameter of about 3 mm. It was then directed into a HurryScan II galvo scanning system with a 100 mm focal length f-θ telemetric scan lens giving a beam diameter on the work surface of about 50 um. Scan speed and laser pulse repetition rate (PRF) were varied depending on the type of experiment being performed, however typical values were 1 m/s scan speed and 20 kHz PRF. For the key parts of this work, the substrate was oriented so that the laser beam was first incident on the TCO film and the distance between the focusing lens and the sample was adjusted so that the beam waist was coincident with the top surface of the sample.

2.3 SUBSTRATE: STRUCTURE OF TEC GLASS

The material used in this experiment was standard TEC 10 glass from Pilkington cut into 2.5”x3.0” squares. The film stack structure is shown in Figure 9 (7). For the depth selective ablation described here the beam impinges from the film side of the substrate as shown.

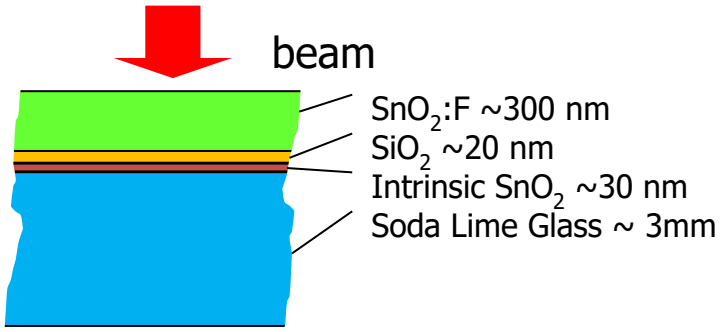

FIGURE 9: MULTI-LAYER STACK STRUCTURE TYPICAL OF TEC15 GLASS. THE SnO_2:F LAYER IS RESPONSIBLE FOR THE HIGH ELECTRICAL CONDUCTIVITY. THE TEC10 GLASS USED IN THESE EXPERIMENTS HAS A SIMILAR STRUCTURE BUT WITH A THICKER SnO_2:F LAYER.

2.4 EQUIPMENT

This work utilized the following metrology equipment:

1. Optical microscope up to 1000x
2. Zygo white light surface profilometer
3. EDX equipped SEM

3.0 PRELIMINARY EXPERIMENTATION

3.1 DEPENDENCE ON WAVELENGTH AND SUBSTRATE ORIENTATION

The laser pulse programmability was used to make an initial survey of the available laser parameter space. Table 1 below shows the initial experimental matrix. The data indicate that scribe depth control could not be achieved for both 532 and 1064 nm with the beam impinging on the glass side of the substrate. We find that under this scenario even very low pulse energies remove the film stack in its entirety. Shorter pulse durations tend to result in pitting of the glass substrate and longer pulses tend to result in the development of micro-cracks in the glass substrate. Figure 10 shows the result of single, 15 µJ, 2 ns pulse interactions with the film stack on TEC10 glass. In contrast with glass side processing, film side processing gives promising results for 532 nm and even more interesting results for1064nm.

TABLE 1: PRELIMINARY EXPERIMENTAL MATRIX.

Pulse Duration 2, 25, 50, 100, 200, 400 ns	Pulse Energy
532 nm Film Side	5 - 50µJ
532 nm Glass Side	5 - 50µJ
1064 nm Film Side	5 - 50µJ
1064 nm Glass Side	5 - 50µJ

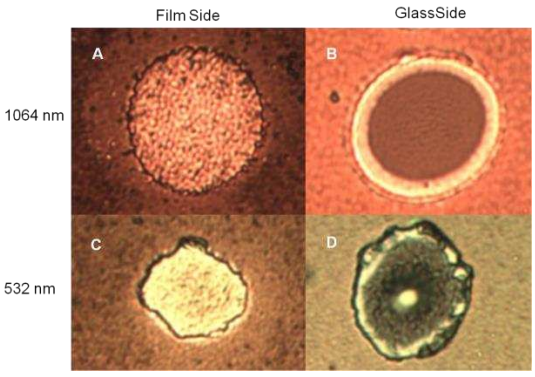

FIGURE 10: SINGLE 15 µJ, 2NS PULSE-FILM INTERACTION MORPHOLOGY. A) 1064 NM FILM SIDE INTERACTION, PIT DEPTH STOPS WELL SHORT OF GLASS SUBSTRATE. B) 1064 NM GLASS SIDE INTERACTION, PIT DEPTH EXTENDS TO AND STOPS AT GLASS INTERFACE. C) 532 NM FILM SIDE INTERACTION, PIT STOPS NEAR GLASS INTERFACE, SnO_2:F LAYER APPEARS TO BE EXPLOSIVELY REMOVED. D) 532 NM GLASS SIDE INTERACTION, SnO_2:F LAYER IS EXPLOSIVELY REMOVED AND A CONICAL PIT HAS FORMED IN THE GLASS SUBSTRATE ITSELF.

3.2 PIT MORPHOLOGY FOR 1064 NM FILM SIDE ABLATION

At 1064 nm we observed two intriguing film side results. First, we find that at short pulse durations a single pulse appears to remove a very specific depth of the SnO_2:F layer. Secondly the bottom of the resulting ablation pit is flat although the spot irradiance profile is nominally Gaussian. Figure 11 and Figure 12 illustrate this phenomenon showing difference in ablation pit depth and appearance for three pulses of identical energy and different durations. Based on these observations, we speculated that removal of the SnO_2:F with 1064 nm is a time dependent phenomenon that may permit very accurate etching of the SnO_2:F layer by controlling the duration and the temporal shape of the laser pulse (8).

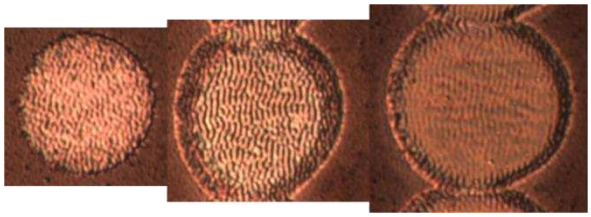

FIGURE 11: APPEARANCE OF PIT BOTTOM WITH INCREASING PULSE DURATION. LEFT, 2NS PULSE SHOWS TEXTURED MORPHOLOGY, 4 NS (MIDDLE) AND 6 NS (RIGHT) SHOW WHAT APPEAR TO BE STANDING WAVE PATTERNS. THE DIAMETER OF THE LEFT PIT IS ABOUT 25 UM.

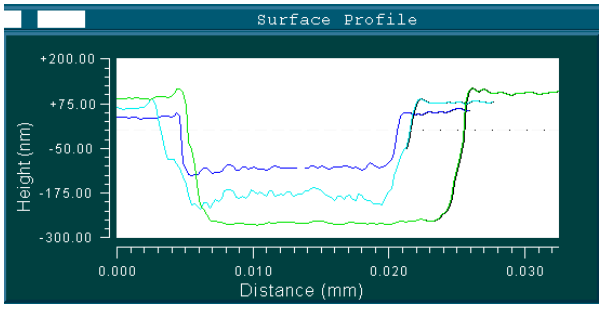

FIGURE 12: PROFILOMETRY INDICATING THAT THE BOTTOM OF THE PIT IS SUBSTANTIALLY FLAT IN SPITE OF THE GAUSSIAN IRRADIANCE PROFILE OF THE BEAM. THE DARK BLUE TRACE CORRESPONDS TO THE LEFT IMAGE OF FIGURE 3, THE LIGHT BLUE TO THE MIDDLE IMAGE AND THE GREEN TRACE TO THE RIGHT.

4.0 FILM SIDE SNO_2:F REMOVAL PROCESS DEVELOPMENT

4.1 PROCESS TIME DEPENDENCE STUDY

The time dependent nature of this removal process implies that the depth of the pit should be controllable by controlling the pulse duration. To test this, we utilize the pulse programmability of the PyroFlex™ laser to create a series of rectangular pulses of constant energy with duration increasing in 1 ns increments. Figure 13 shows pictorially how the laser pulse duration was changed for the experiment. The resulting pit "etch" depth for each pulse was measured utilizing the Zygo surface profilometer and plotted in **Error! Reference source not found.** The p it depth grows approximately linearly with pulse duration until process reaches the interface between the SnO_2:F and the next layer (SiO_2) layer. At the interface, there is a clear transition and reduction in "etching" rate. The slope transition depth matches the published thickness of the SnO_2:F layer which is typically about 370 nm.

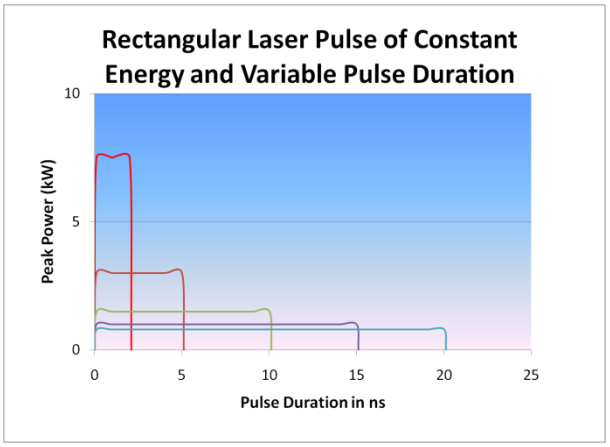

FIGURE 13: CARTOON DEPICTING HOW THE RECTANGULAR LASER PULSE DURATION WAS VARIED AT CONSTANT TOTAL PULSE ENERGY FOR GENERATING THE DATA IN FIGURE 14.

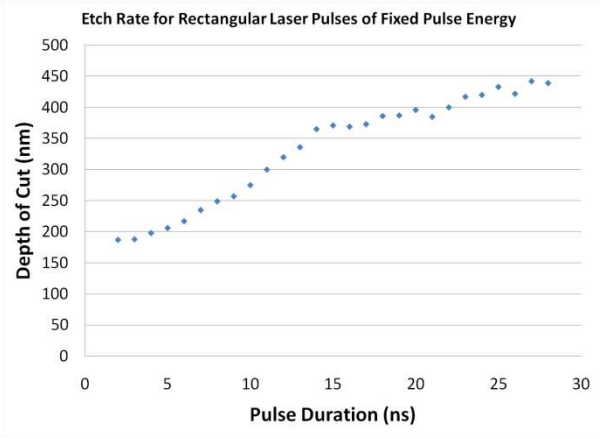

FIGURE 14: PIT DEPTH AS A FUNCTION OF PULSE DURATION FOR RECTANGULAR SHAPED PULSES. NOTE THE CHANGE IN SLOPE AT THE SiO_2 / SnO_2:F INTERFACE.

4.2 PIT DEPTH AS A FUNCTION OF PULSE ENERGY

As the next step in this study we characterized the evolution of pit formation with time for both fixed peak power and fixed pulse energy. For a square temporal pulse shapes (as in Figure 15) of constant peak power, the total pulse energy increases in proportion to the pulse duration. Therefore, the red trace in Figure 15 represents a 5-fold increase in the pulse energy with pulse duration from 2 to 10 ns (15 to 75 µJ). The green trace on the other hand is fixed at 15 µJ for all pulse durations. This test gave a peculiar result. As Figure 15 clearly demonstrates, the pulse energy has little if any impact on the depth of the pit. The overall pulse duration appears to be the only important variable for determining the depth of the resulting pit. Figure 16, however, illustrates that the diameter of the pit is quite strongly dependent on total energy and only weakly dependent upon peak power, implying a threshold-based process in energy density (J/cm^2). The implication of this data is that the process is initiated by crossing an energy density threshold, but rate limited since additional energy does not result in a deeper pit or change in the pit morphology. We can also infer that the process is rapidly quenched upon cessation of the laser pulse. A possible explanation for this result is that the process at work is endothermic chemical reaction since it terminates as soon as the incident energy is removed.

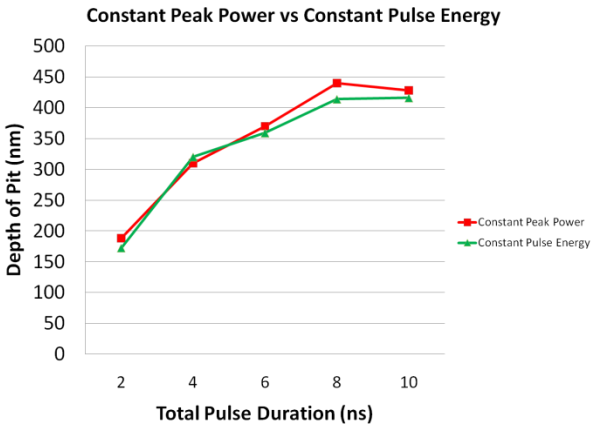

FIGURE 15: IMPACT OF PEAK POWER AND PULSE ENERGY ON DEPTH OF SINGLE ABLATION PITS. DATA INDICATES THAT THE PROCESS IS INDEPENDENT OF PEAK POWER AND TOTAL ENERGY OVER THE RANGE EXAMINED. THE ONLY VARIABLE THAT CORRELATES WITH THE DEPTH OF THE PIT IS OVERALL PULSE DURATION.

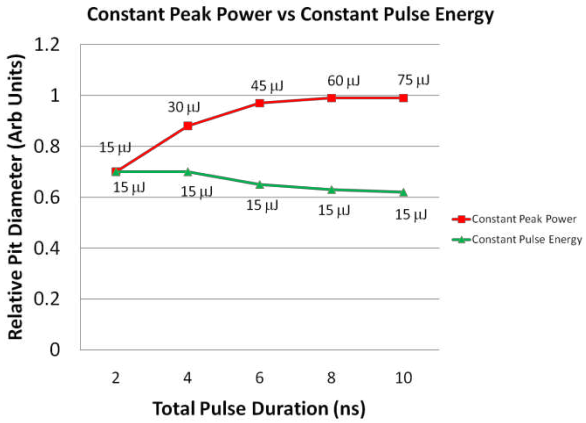

FIGURE 16: EFFECT OF ENERGY DENSITY ON PIT DIAMETER. PROCESS SHOWS STRONG DEPENDENCE ON TOTAL ENERGY DENSITY BUT ONLY WEAK DEPENDENCE ON PEAK POWER.

4.3 ENERGY THRESHOLD FOR PIT DEPTH GROWTH

Since we observed that once initiated this material removal process proceeds at a constant rate independent of pulse energy we postulated that reducing the energy content of the pulse after initiation could yield a valuable insight regarding the physical mechanism at work. To test this postulate, we constructed a set of “chair” shaped laser pulses. The goal was to find the minimum peak laser power required to sustain the interaction. With a fixed amount of pulse energy, half of it always in the leading 2 ns of the pulse and half always in a fixed intensity tail of variable duration, we performed a series of experiments depicted in Figure 17 (right) over a range of total pulse energies.

Figure 17 (left) illustrates the how the “chair” shape of the laser pulse was varied for each of the experiments. As before, we examined the resulting pits from the interaction of a single laser pulse with the substrate.

We confirmed that for the 2ns pulse with no tail, the pit depth was independent of pulse energy (trace 1). The addition of a 4 ns tail (Pulse 2), shows an increased pit depth with only weak and slightly inverse energy dependence (trace 2). Laser pulse #3, with a 2 ns leading edge followed by an 8 ns tail, shows a puzzling inverse relationship to pulse energy. The depth of the ablation pit decreases substantially with pulse energy. At this point we do not have an explanation for the physical mechanism behind this behavior. For laser pulses 4 and 5 with the longest tail durations we see that all the material has been removed although the peak power in the tail has dropped to only 12% and 6% of the initial peak power respectively. Overall, this behavior points to a material removal process that, once initiated, requires very little energy input to keep it going.

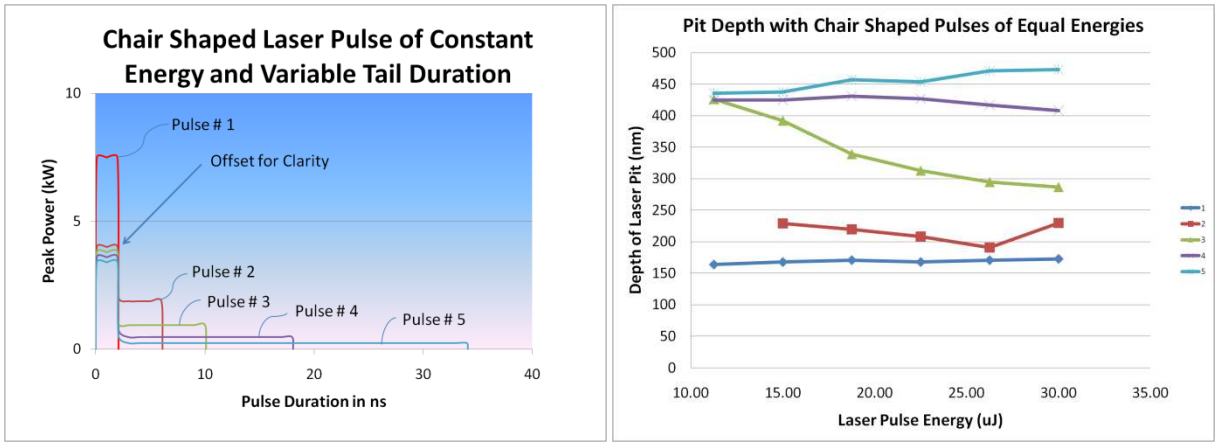

FIGURE 17: (LEFT) CARTOON DEPICTING 5 DIFFERENT CHAIR SHAPED PULSES. (RIGHT) RESULTING PIT DEPTH FROM SINGLE LASER PULSE-FILM INTERACTIONS FOR THE VARIOUS CHAIR SHAPED LASER PULSES DEPICTED IN THE TOP FIGURE.

To compare the chair shape pulse result with the rectangular laser pulse shape result, we modified the pulse duration vs pit depth test shown in Figure 17. In this experiment, we used a “chair” pulse with a “seat” that was only 3% as high as the initial 2 ns leading edge and we varied the duration of the chair “seat” with a fixed chair “back” of 2 ns. Total energy was allowed to increase as the “seat” was lengthened, with a total increase in energy of 30% as the “seat” was increased from 0 to 22 ns. Figure 18 shows the comparison between the rectangular pulse shape result and the chair pulse shape result. Figure 19 shows how the morphology of the ablation pit

evolves as the “seat” is lengthened. The striking feature is that despite significant differences in the distribution of energy between the “back” and the “seat”, the pit depth increases in a systematic fashion. Of special interest is the fact that the SiO_2 and SnO_2 barrier layers are reached at consistent overall pulse duration. Again this is a strong indicator the material removal mechanism at play is rate limited and requires activation for about 15 ns to remove all SnO_2:F down to the SiO_2 layer. Furthermore, once activated, the removal mechanism requires only about 3% of the initial activation peak power to sustain itself. It is our supposition that this behavior indicates either a thermally driven phase change of the material or a thermally initiated chemical dissociation. A final detail to not is that once the SiO_2 layer is reached the removal of the final SiO_2 and intrinsic SnO_2 layers no longer occurs in a linear manner independent of peak power. We can see that beginning at about 10 ns the center area thins more quickly than the edges, possibly indicating that the process that removes the last two layers is fundamentally different than the process that removes the SnO_2:F layer.

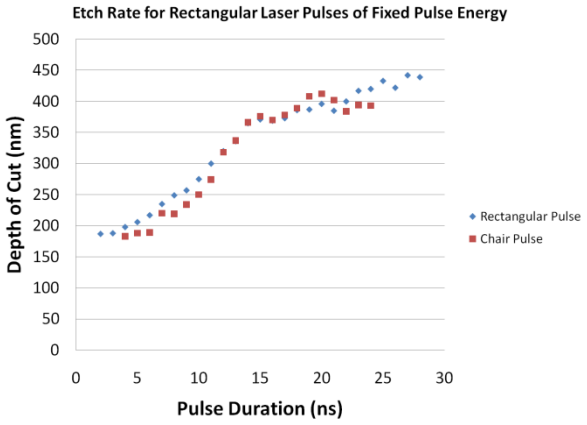

FIGURE 18: ETCH DEPTH VS. PULSE DURATION FOR A RECTANGULAR LASER PULSE COMPARED TO ETCH DEPTH VS. “SEAT” DURATION FOR A "CHAIR" SHAPED PULSE. RESULTS ARE NEARLY IDENTICAL DESPITE A LARGE DIFFERENCE IN PEAK POWER.

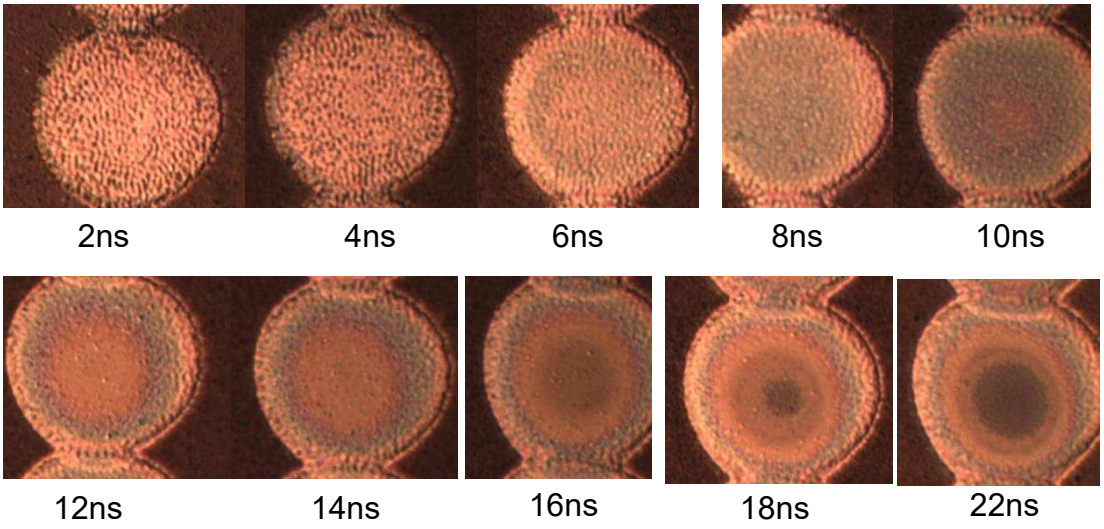

FIGURE 19: OPTICAL MICROSCOPY OF THE EVOLUTION OF PIT MORPHOLOGY WITH INCREASING "CHAIR" PULSE "SEAT" DURATION. AT ABOUT 12NS THE SnO_2:F APPEARS TO BE REMOVED AND AT ABOUT 18 NS THE REMAINING SiO_2 AND SnO_2 LAYERS ARE PENETRATED.

4.4 ORIGIN OF SURFACE MICROSTRUCTURE.

Another curious feature of this material removal mechanism is clearly seen in the pit morphology. Although the irradiance profile is spatially Gaussian, the bottom of pit is substantially flat with an appearance that changes from granular in texture to a texture that appears to have characteristics of a consistently aligned standing wave pattern. Other groups have reported similar standing wave patterns associated with ablation pits created with ps and fs laser sources (9), (10), (11) and the phenomenon appears to be universal across many different materials. The most common explanation appears to be that interaction of the beam with periodic or random features of the sample induce interference effects that ultimately modulate the laser intensity at the surface and hence create the microstructure. This does not seem a fully satisfactory explanation however since these materials are amorphous and general smooth on optical scales.

An insightful fact that we observed is that this pattern is dependent upon the polarization of the incoming beam. The ripple was found to orient itself along the axis of polarization. This orientation dependence was observed both directly under a 1000x microscope as well as indirectly by observing the resultant angular dependency in diffractive effects (Figure 20). For left and right circular polarization we found ripple patterns that aligned at 45 degrees to the two orthogonal polarizations. This dependence on the electric field vector orientation has interesting implications. It may be possible that the periodic structure observed is due to resonance of the free electrons with the beam electric field. The electron oscillation may set up an out of phase electromagnetic field that forms a beat pattern with the incident beam. Other studies have implicated interference with the substrate crystal lattice as the source of the interference effects but in this case the material is nominally amorphous. Whatever the origin of this microstructure, we observe that the periodicity results in a strong grating effect. So much so that the glass surface can be induced to have a colored appearance depending on viewing angle. Furthermore, the apparent color, and by proxy, the grating period is observed to be a function of pulse duration.

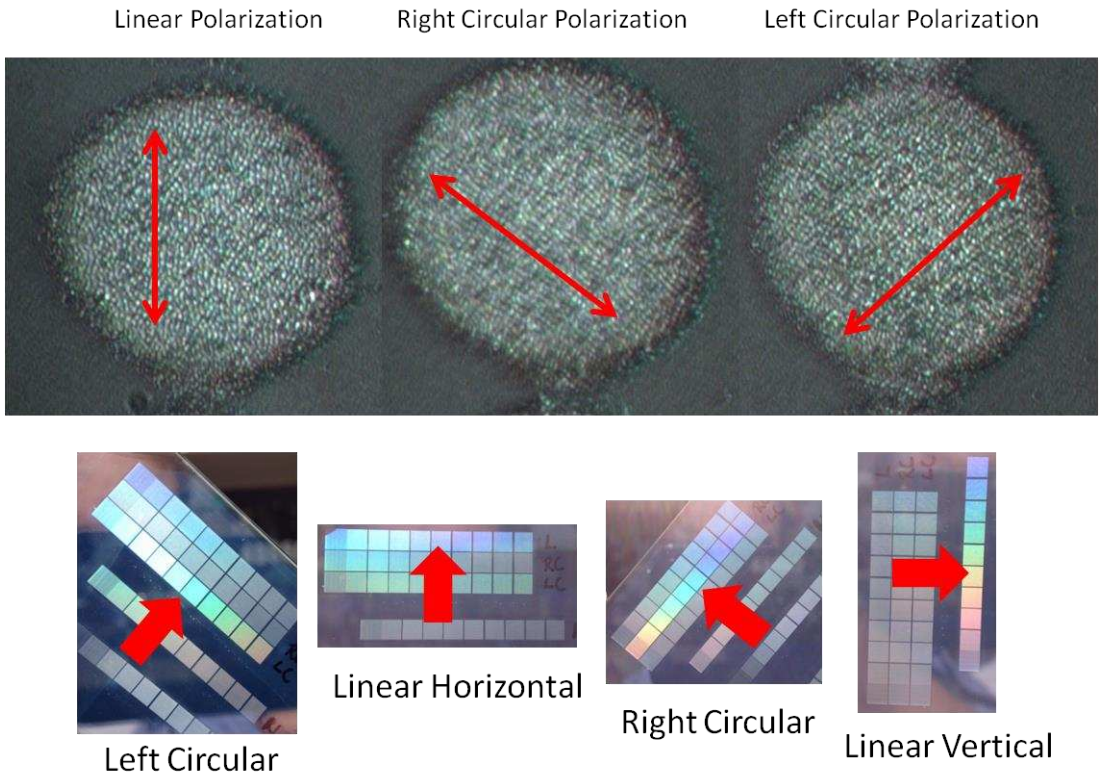

FIGURE 20: ORIENTATION OF SURFACE MICROSTRUCTURE DEPENDING UPON POLARIZATION OF THE INCOMING BEAM (RED ARROWS: TOP). (BOTTOM) ARRAYS OF ABLATION SPOTS ARE WRITTEN INTO 4 MM SQUARE BOXES IN ORDER TO CREATE A BULK DIFFRACTION EFFECT THAT IMPARTS AN APPARENT COLOR TO THE FILM. THE COLOR EFFECT IS STRONGLY DEPENDENT UPON THE ORIENTATION OF THE SUBSTRATE RELATIVE TO THE VIEWER AND THE ORIENTATION OF THE OPTIMAL COLOR EFFECT IS DEPENDENT UPON THE POLARIZATION OF LIGHT USED.

5.0 PROPOSED PROCESS PHYSICS

5.1 IMPLICATIONS OF OBSERVATIONS

At this point it is useful to recap the relevant features of this material removal mechanism. They are:

1. Pit depth is independent of pulse energy and peak power.
2. Bottom of pit is flat despite Gaussian irradiance profile.
3. Overall pit depth is a nearly linear function of pulse duration.
4. Pit diameter is a strong function of pulse energy but not peak irradiance.
5. Process appears to immediately halt up cessation of the pulse.
6. Once initiated, the process is sustained even when peak irradiance is reduced by 97%
7. Other than surface microstructure, the bulk of the SnO_2:F seems to be unaffected by the process.

5.2 ABSORPTION MECHANISM

First, we have observed that the material is highly transparent at 1064 nm. So much so that for a low power beam there is no noticeable attenuation in the film. The interaction is therefore likely driven by the nonlinear effects at the very high irradiance of the beam spot. Furthermore, unlike the 532nm result where the interaction appears to initiate at the interface between film and glass substrate, the 1064 nm interaction initiates at the outside surface and grows deeper into the SnO_2:F film with time. A clue to this behaviour can be found by comparing the film side and the glass side results as shown in Figure 10. We can see that in both cases the reaction appears to have initiated at the first of the SnO_2:F surface the beam encounters. When the surface is the interface between the glass and the SnO_2:F, the SnO_2:F film is completely removed at even the shortest pulse duration whereas when the first interface is between air and SnO_2:F the time dependant material removal occurs.

Next, we must consider that the material is an N-type doped semiconductor (5) . The material is transparent to visible light because it has a very large band gap > 3.6 eV but at the same time is a conductor because of a populated conduction band. While we have no direct evidence, it seems reasonable to assume that high irradiance would tend to populate any inter-band defect surface states resulting in nonlinear absorption. Alternatively, the photon energy at 1.17 eV of the laser at 1064 nm may excite intra-band transitions. Whatever the mechanism it

seems that under high irradiance at 1064 nm there is significant absorption at the first SnO_2:F interface encountered by the beam. Two interesting experiments would be to repeat the tests with intrinsic SnO_2 to observe if the same surface absorption phenomenon presents itself and measure the reflected fraction of the beam as a function of intensity. If free carriers in the conduction band are important than we might expect the material to behave more as a mirror and for reflectivity to increase whereas with intrinsic SnO_2 having an unpopulated conduction band might be expected to not exhibit the same behaviour.

5.3 SNO_2 PHYSICAL PROPERTIES

One interpretation of these observations suggest that a chemical dissociation of the SnO_2:F layer is occurring. A calculation based on the enthalpy of formation for SnO_2 indicates that it should take about 4μJ of energy to dissociate the volume of SnO_2 present in a single 25μm diameter pit from a single pulse interaction (Table 2). Recognizing that this calculation does not include the heat capacity, heat of fusion, or heat of vaporization, this is not inconsistent with the actual energy (15μJ) delivered in the laser pulse. Furthermore, the dissociation reaction is endothermic which means as soon as the heat source is removed, the reaction will cease (12). This compares favorably with the fact that very little energy input is required to sustain the process and that the process terminates as soon as the energy input is discontinued.

TABLE 2: SNO2 THERMODYNAMIC PROPERTIES.

Enthalpy of Formation for SnO2 (12)	-577	kJ/mol
Typical Pit Volume (fully removed)	1.36E-10	cm^3
Density	6.95E+00	gm/cm^3
Mass	9.43E-10	gm
Molar Mass	150	gm/mol
Mole	6.29E-12	mol
Energy Released in Formation	4	μJ

It is more difficult to understand why the reaction proceeds uniformly despite the non-uniform intensity profile of the irradiating beam. However, one clue comes through examining the material behavior in the far IR. The most common application for TEC glass is as far infrared reflectors for heat reflecting windows. This high reflectivity is known to arise due to interaction of far IR photons with electrons in the conduction band (13). Furthermore,

higher electron mobility is associated higher electrical conductivity and with higher optical reflectivity at shorter wavelengths (14). It reasonable to suppose that the intense oscillating electric field at the laser focus would have the effect of simultaneously promoting valence band electrons to the conduction band via defect states and promotion of conduction band electrons to more loosely bound conduction band states. In the extreme case, these conduction band electrons may become free electrons initiating the evolution of the plasma generation and ablation classically associated with laser ablation events. However, since we do not observe explosive ionization driven ablation we infer that ionization and ejection of electrons occurs only weakly or perhaps not at all.

Increased population of electrons in the conduction band and promotion of existing electrons to more loosely bound energy levels will increase the film conductance and mobility of the electrons. There are two clear effects that will occur as carrier concentration in the conduction band is increased and defect states are filled. First, optical absorption of the sample will increase (15). However, at the same time the reflectivity of the material should shift to shorter wavelengths as the higher mobility allows the electrons to respond resonantly to higher frequency electric fields. At this point we have no means to characterize these effects however we can analyze the observed material behavior and compare it to these two models.

As noted we observe that the laser interaction proceeds from the surface (top 50 nm) into the bulk of the material with no apparent damage to the underlying bulk material (bulk meaning ~250 nm remaining film thickness). If the immediate effect of the impinging laser energy was an increase in the absorption coefficient one would expect large energy deposition throughout the bulk of the film. As we have shown however, there is about 4 times more energy available in the laser pulse than would be required to completely dissociate the entire volume of the film, yet we observe what is effectively a surface interaction that does not change its character even with very large changes in pulse energy. This observation is not consistent with the idea of bulk effects in the semiconductor.

Amalric-Popescu et al (15) showed that surface states and adsorbed species played a key role in determining the reflectivity and absorptivity of SnO_2 films. Furthermore, it makes sense that defect states would be more common on the surface of the material than in the bulk. Hence the surface of the film would respond more strongly to the

incident radiation. The sudden increase in conduction band carrier concentration would then initiate a cascade that both increases absorption and reflectivity of the surface. This would reduce the energy density in the bulk thereby protecting it from damage and cause a rapid increase in temperature at the surface.

The melting point of SnO_2 is reported as 1630 C and the boiling point is reported to be between 1800 and 1900 C with chemical dissociation reported at 1900 C (16). With these reference points a potential mechanism for this ablation mechanism becomes clear, namely, that the surface interaction causes a chemical dissociation originating at the surface that progresses into the bulk as the duration of the interaction increases. Even with this mechanism it is difficult to understand how the pit depth can grow linearly independent of the intensity profile. If the transport mechanism is thermal conduction, the reaction front would progress more quickly where the thermal gradient was highest but this is clearly not the case. One possible explanation then is that this process unfolds at a faster rate than the thermal conduction time. This possibility is supported by the observation in previous work that when the pulse duration approaches 1 ns in silicon, material removal rates drop dramatically for classic laser ablation (17). Confirmation of this idea requires further study.

5.4 PROPOSED MATERIAL REMOVAL MECHANISM

We believe that the material removal mechanism can be encapsulated in the following model:

1. Defect states at the surface interact with the high intensity of the electric field to increase both the population and energy of the electrons in the conduction band.
2. Increased population of the conduction band increases the electron mobility which increases the reflectivity of the surface at shorter wavelengths. At the same time the surface absorption coefficient is increased.
3. These two effects reduce the intensity of the optical radiation in the underlying SnO_2 and increase the temperature at the surface.
4. The surface temperature rapidly reaches the thermal decomposition temperature for SnO_2 yielding Sn and O_2 gas.

5. Once the process is initiated, it can be sustained by continuing to add a small amount of energy to maintain the surface temperature above the SnO_2 dissociation temperature. Figure 21 below illustrates how this can occur. An initial pulse of light raises the temperature at the surface to the dissociation point for SnO_2. Once the process is initiated, the laser intensity only needs to be high enough to replenish the heat lost to radiation and absorbed by the endothermic dissociation. Thermal conduction is assumed to be negligible on this time scale.

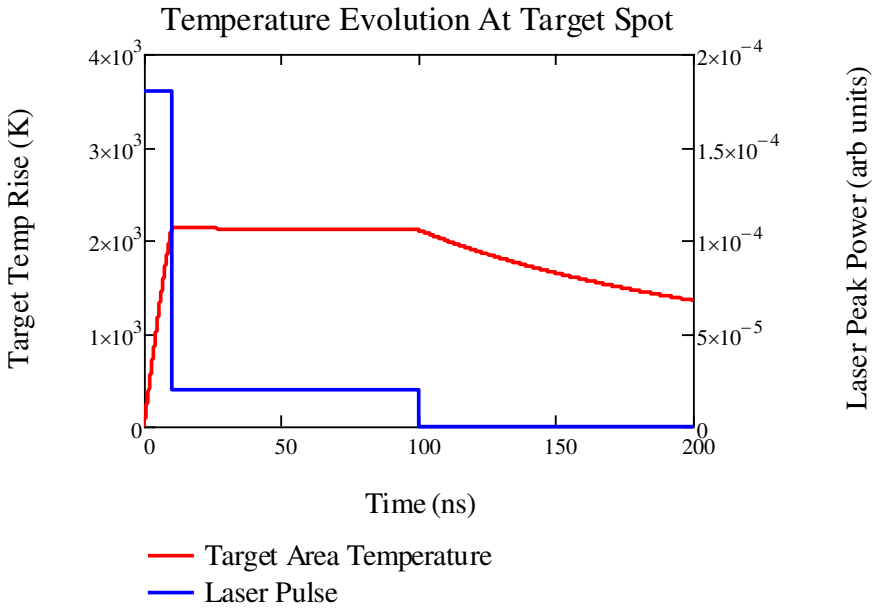

FIGURE 21: ILLUSTRATION OF THE CONCEPT OF INITIATING THE SnO_2 REMOVAL MECHANISM WITH AN INITIAL HIGH INTENSITY PULSE AND SUSTAINING IT WITH A LOWER INTENSITY PULSE.

6.0 APPLICATION TO CDTE P1 SCRIBE PROCESS

6.1 CONTINUOUS SCRIBES

Until this point, this study has examined the results of single laser pulse interactions with the substrate. However, for a successful P1 laser scribe, the individual laser pulses must be overlapped to produce a continuous scribe line. We must consider the possibility that "double dosing" in the spot overlap region will damage or destroy the SiO_2 and SnO_2 barrier layers. Furthermore, the electrical resistance of the scribe must be very high to produce a useful solar cell structure.

To verify that pulse overlap would not periodically puncture the SiO_2 layer when continuous scribes were produced, we created continuous scribes of varying overlap utilizing the ideal pulse configuration found for single spot ablation and compared them to scribes made with very high energy and pulse duration that remove all material. It was found that maintaining the spot overlap around 30% did not breach the barrier layers as indicated in Figure 22. Optical microscopy also indicates that at 15 ns chair duration, the barrier layers are intact as shown in Figure 23. Furthermore, we find that the resistance across the resulting scribe also increases with increasing "seat" duration reaching a plateau of about 100 kΩ for a 15 ns "seat" duration pulse, a 25µm wide groove, and a 10 mm length. The beginning of this resistance plateau corresponds precisely to the time at which the SiO_2 layer is reached. Together, Figure 24 and Figure 25 illustrate the relationships between the "seat" duration of the "chair" pulse, the depth of the resulting scribe, and the resistance of the scribe as measured with a simple digital volt meter.

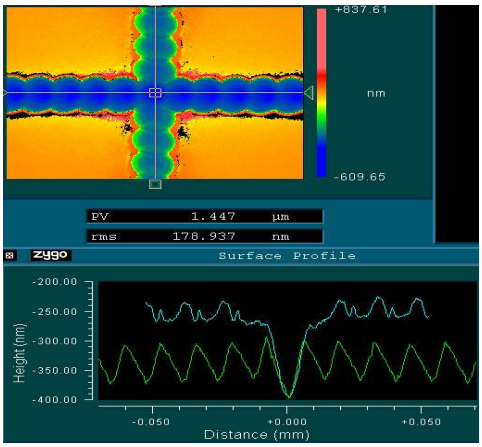

FIGURE 22: HORIZONTAL SCRIBE AT TOP (GREEN PROFILE AT BOTTOM PLOT) INDICATES SCRIBE WHERE ALL LAYERS ARE REMOVED. VERTICAL SCRIBE AT TOP (BLUE PROFILE AT BOTTOM PLOT) INDICATES WHERE ONLY SnO_2:F LAYER IS REMOVED. THE DIFFERENCE IN DEPTH BETWEEN THE TOP AND BOTTOM CURVE IS ABOUT 50 NM AND CORRESPONDS TO THE THICKNESS OF THE BARRIER LAYERS INDICATING THAT THEY HAVE NOT BEEN BREACHED.

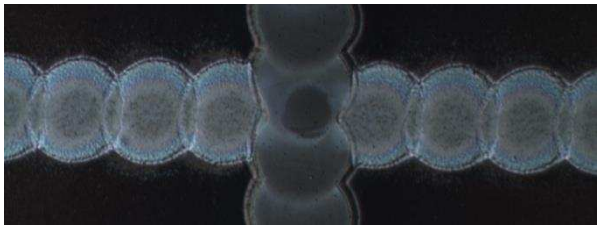

FIGURE 23: VERTICAL SCRIBE IS PERFORMED UNDER AGGRESSIVE LONG PULSE DURATION CONDITIONS THAT REMOVE ALL LAYERS FROM TCO STACK. THE HORIZONTAL SCRIBE IS PERFORMED WITH A "CHAIR" SHAPED PULSE WITH "SEAT" DURATION OF 15 NS. THE PICTURE CLEARLY INDICATES THAT THE BARRIER LAYERS ARE LARGELY INTACT.

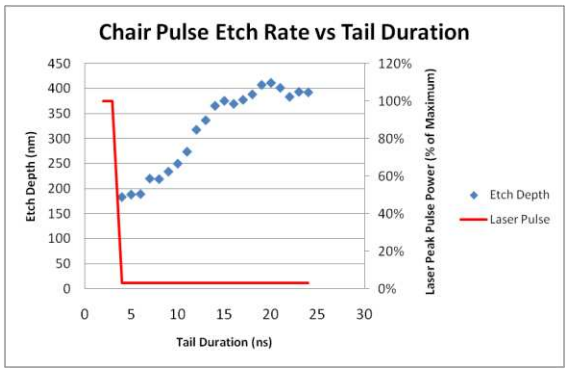

FIGURE 24: LASER INPUT ENERGY PROFILE (RED- RIGHT AXIS) AND RESULTING PIT DEPTH VS TIME (BLUE LEFT AXIS). THE CHANGE IN SLOPE OF THE BLUE CURVE AT ABOUT 360 NM DEPTH CORRESPONDS TO AN ETCH RATE CHANGE THAT OCCURS AT THE SnO_2:F – SiO_2 INTERFACE. THE "TAIL DURATION" INCLUDES THE INITIAL 2NS HIGH PEAK POWER SPIKE.

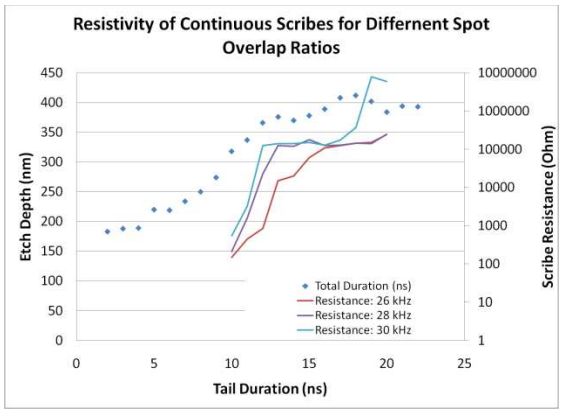

FIGURE 25: RELATIONSHIP BETWEEN ETCH DEPTH (BLUE – LEFT AXIS), SCRIBE RESISTANCE (SOLID CURVES – RIGHT AXIS) AND "CHAIR" PULSE "SEAT" DURATION (HORIZONTAL AXIS) FOR THREE DIFFERENT SPOT OVERLAPS. NOTE HOW THE PLATEAU IN SCRIBE RESISTANCE CORRESPONDS TO THE CHANGE IN ETCH RATE WHEN THE SnO_2:F – SiO_2 INTERFACE IS REACHED.

6.2 DISCUSSION

While the resistance of the scribes has been shown to be very high (>100 kΩ for a 10 mm scribe), typical P1 scribes are expected by manufacturers to be in the 10's of MΩ. It is not clear if the residual conductivity is the result of residue left in the scribe bottom or possible changes in the structure of the 30 nm thick intrinsic SnO_2 layer. While the measured resistance should be more than sufficient for efficient solar modules, the origin of the residual conductivity and strategies to eliminate it will be a central part of future study.

The physical evidence suggests that the barrier layers remain intact, however it is necessary to test the ability of the laser processed layers to resist Na diffusion directly. The next section focuses examining the electro-migration of Na directly. We also had plans to construct optimized mini-modules and evaluate the module performance relative to controls under accelerated life test conditions. Changes in the business conditions that drove this program combined with a disappoint first result unfortunately prevented this follow-on work.

Finally, for reference the real physical pulse shape that was found to be optimal and utilized for all subsequent processes is captured below in Figure 26.

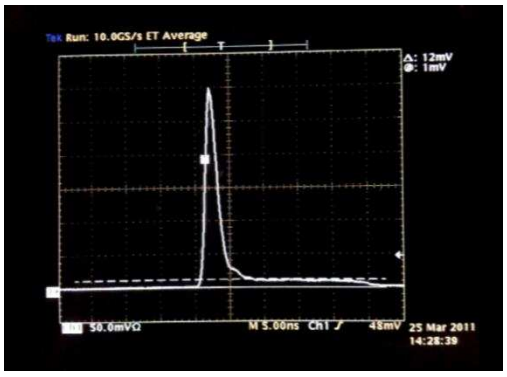

FIGURE 26: ACTUAL CHAIR SHAPED PULSE AS OBSERVED ON A PHOTO-DIODE. VERTICAL AXIS IS PEAK OPTICAL INTENSITY AND HORIZONTAL IS TIME IN NS.

6.3 SODIUM DIFFUSION TEST OVERVIEW

To test the viability of this process as a P1 scribe a standard test was needed. Abound solar had developed a standard test protocol for evaluating the resistance of the P1 scribe. The exact details of this test were considered

proprietary to Abound solar and I was unfortunately not allowed to inspect the test apparatus or to know details of how the test was performed. However, generally the test protocol is as follows:

1. The P1 sample is prepared.
    a. CdS/CdTe layers are deposited on the TEC10 glass substrate.
    b. Laser is used to make the P1 scribe.
    c. Scribe groove is filled with photoresist.
    d. Panel is cleaned.
2. The sample temperature is raised to 80C.
3. 750 Volt is applied across the scribe in question.
4. The resistance of the scribe is measured as a function of time.
5. Degradation of the scribe resistance is assumed to directly proportional to diffusion of Na into the scribe and the surrounding semi-conductor.

For the samples produced with this novel P1 process the protocol was modified as follows

1. 3.5x4.0 inch samples were provided to ESI by NSF I/UCRC.
2. The new P1 scribe process was applied at ESI with variable process conditions.
3. Samples were returned to NSF I/UCRC for CdS and CdTe deposition.
4. The samples were passed to Abound solar to perform the Na diffusion test.
5. The remainder of the process was unmodified.

It is worthwhile to note that at this point in the process the structure of the our modified cell is fundamentally different than the standard cells. Specifically, in the standard process the P1 scribe filled with photoresist completely separates the two cells. In our modified process, the P1 scribe is bridged by the CdS/CdTe layers. Figure 27 below pictorially illustrates the structural difference between the standard cells that the Abound test was designed for and our modified cells with the CdS/CdTe layers shunting the scribe. At first glance this would appear to mean that the cells would be electrically shunted and the test invalid. However it was the position of CSU and Abound personnel that because the sheet resistance of the CdS/CdTe layers was very high that the test would still

be valid and the resistance between adjacent cells would not be largely impacted. The assumption that the test remains a valid comparison between the standard and modified processes however remains invalidated.

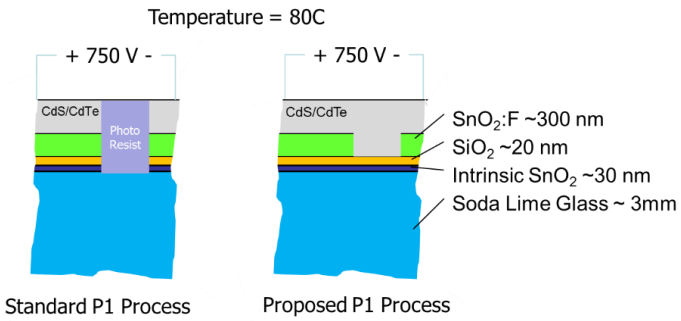

FIGURE 27: COMPARISON OF STANDARD AND PROPOSED P1 STRUCTURE FOR NA DIFFUSION TESTING.

6.4 SAMPLE PREPARATION

10 test scribes were prepared on each of two 3.0 x 3.6 " TEC 10 substrates. The test scribes were designated R1 through R10 and the conditions were identical for both samples. The scribes divided each substrate into 11 electrically isolated pads as shown in Figure 28.

Table 3 below summarizes the various test conditions applied.

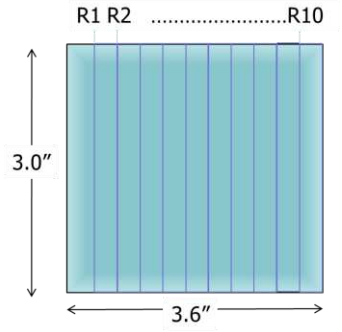

FIGURE 28: LAYOUT OF TEST SCRIBES FOR P1 NA DIFFUSION TESTS.

TABLE 3: LASER SCRIBE CONDITIONS FOR NA DIFFUSION TESTS. (NOTE, THESE ARE FROM MEMORY, NEED TO FIND LAB BOOK AND CONFIRM)

Scribe Reference	Initial Pulse Duration (ns)	Pulse Tail Duration (ns)	Pulse Energy uJ	Repetition Rate kHz	Scribe Velocity mm/s
R1	10	na	15	28	500
R2	15	na	15	28	500
R3	20	na	15	28	500
R4	25	na	15	28	500
R5	50	na	15	28	500
R6	2	10	15	28	500
R7	2	12	15	28	500
R8	2	14	15	28	500
R9	2	16	15	28	500
R10	2	18	15	28	500

The resistance between adjacent pads (scribe resistance) was characterize immediately after application of the laser scribes utilizing a standard laboratory digital multimeter. The data are shown in Figure 29.

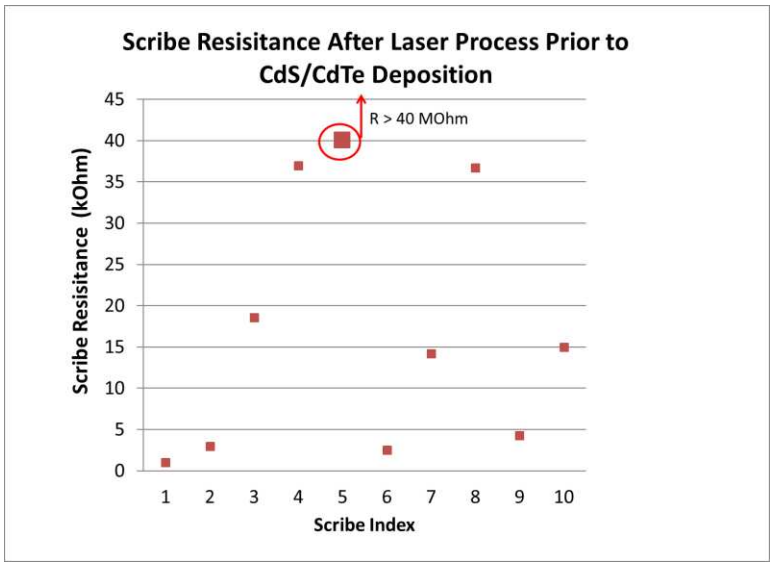

FIGURE 29: SCRIBE RESISTANCE MEASURED IMMEDIATELY AFTER LASER THE LASER SCRIBE PROCESS BEFORE CDS/CDTE DEPOSITION. NOTE THAT THE POINT AT 40KOHM IS 40 MOHM BUT WAS RESCALED FOR CLARITY.

6.5 SODIUM DIFFUSION TEST RESULTS

Next the samples were shipped to NSF I/UCRC where a standard CdS/CdTe deposition was performed. Note that I do not have the details of this process, but my understanding was that the deposition was chosen to be consistent with the production process utilized in standard cells from Abound. After deposition, the samples were then taken to Abound Solar's testing lab where the Na diffusion test was applied. The data output of the Na diffusion test is a measurement of the scribe resistance as a function of time. First, note the comparison of the scribe resistance as measured at the time of laser scribing with that initially measured in the Na diffusion test shown in Figure 30. The first key feature to note is that the initial measurements are on average about a factor of 50 lower in the Na diffusion test measurement compared to the post laser scribe measurement. This feature is already puzzling and means that the starting scribe resistance is already unacceptably low to produce solar panels. In addition to being anomalously low, we can see from Figure 30 that the scribe resistance at the start of the Na diffusion test is uncorrelated with the measurement post laser scribe. We were not able to come up with a compelling explanation for these discrepancies, however it would be worthwhile to reconsider the assumptions that the sheet resistance of the CdS/CdTe layers would not play an important role. Additionally, we did not place controls on the width of the laser scribe, neither did we try to match the scribe width applied in the standard P1 scribe process. In retrospect, the applied scribe width was only about 30 um compared to a scribe with of 60 to 70 um for a standard CdTe P1 scribe (Figure 31). Prior experience with laser scribes on ZnO on glass for amorphous silicon indicate the that the breakdown voltage in air for 30 um scribes is between 250 and 500 V (Table 4). It thus seems very likely that the reason for the initial low resistance measurement was because the scribes were immediately damaged upon application of the 750 Volt potential for the NA diffusion test. Furthermore, it is possible that the test measured the degradation of the scribes due to arcing rather than the diffusion of Na. Were the test to be repeated, the laser scribe width should be increased to be similar to the standard laser scribe width and the voltage used for the test should be reevaluated. Also, I would propose that a standard test control sample should be fabricated utilizing standard P1 processes.

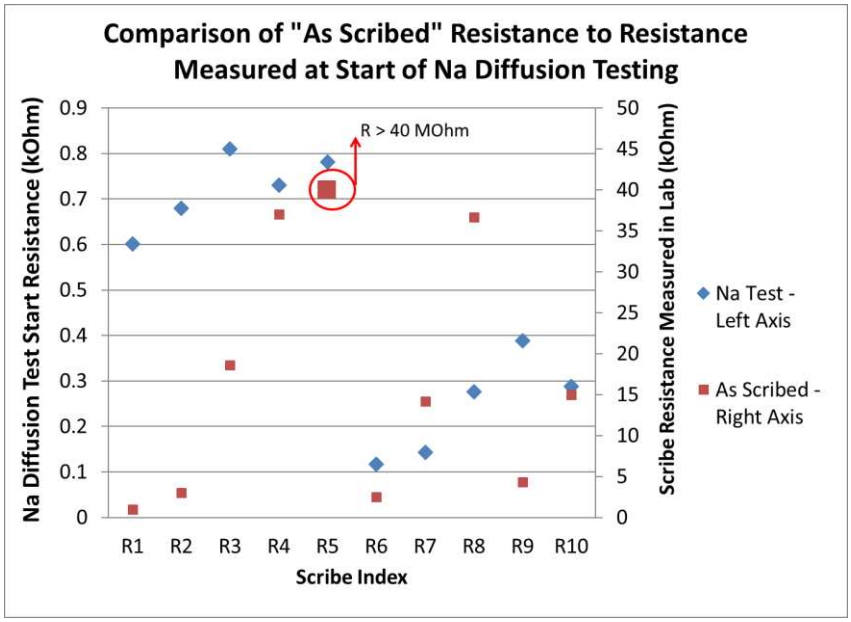

FIGURE 30: COMPARISON OF INITIAL SCRIBE RESISTANCE AS MEASURED AT THE TIME OF THE LASER SCRIBE PROCESS (RIGHT AXIS) AS COMPARED TO THE SCRIBE RESISTANCE AT THE BEGINNING OF THE NA DIFFUSION TEST (LEFT AXIS). (NA DIFFUSION TEST DATA GATHERED BY ABOUND SOLAR, DATA ANALYSIS PERFORMED BY MATT REKOW).

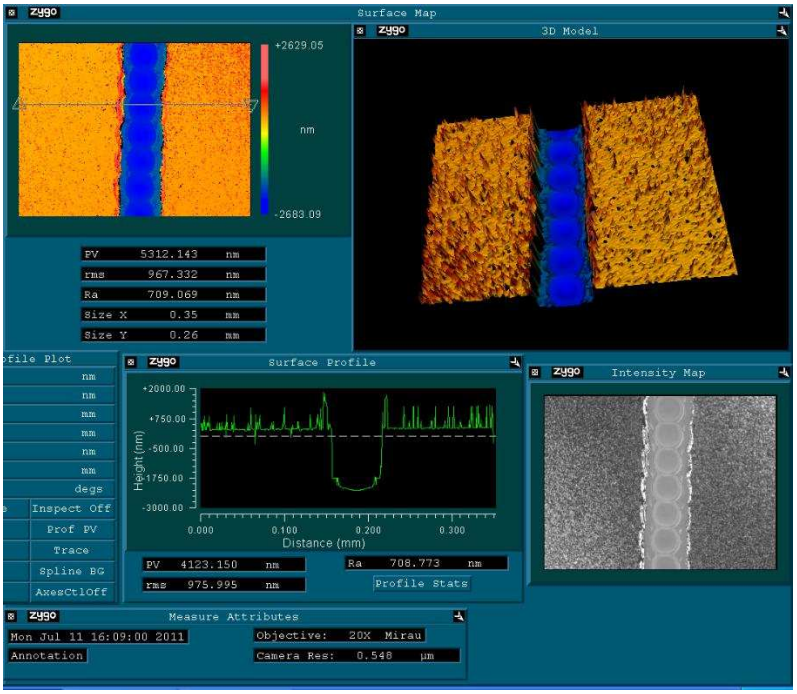

FIGURE 31: MORPHOLOGY OF A STANDARD P1 LASER SCRIBE IN CDTE INDICATING A SCRIBE WIDTH OF ABOUT 70 UM.

TABLE 4: BREAKDOWN VOLTAGE MEASUREMENTS FOR LASER SCRIBES IN ZNO FILMS ON GLASS AS A FUNCTION OF LASER SCRIBE WIDTH. OL INDICATES THAT THE SCRIBE RESISTANCE IS GREATER THAN 200 MOHM, BD INDICATES ARCING ACROSS THE SCRIBE.

Sample Description		Resistance Measurment (Meter Max, 500 Ohm)	125 V (MOhm)	250 V (MOhm)	500 V (MOhm)	1000 V (MOhm)
Groove Width	Overlap					
54 um	10%	>500	OL	OL	BD	
	25%	>500	OL	OL	BD	
	50%	>500	34	BD		
	10%	>500	OL	OL	BD	
	25%	>500	OL	OL	BD	
	50%	>500	OL	OL	BD	
25 um	10%	>500	9.6	BD		
	25%	>500	4.8	BD		
	50%	>500	OL	OL	130	BD
30 um	10%	>500	OL	OL	BD	
	25%	>500	OL	OL	BD	
	50%	>500	OL	OL	BD	
10 um	10%	>500	0.0005	BD		
	25%	>500	0.0014	BD		
	50%	>500	0.0004	BD		
	10%	>500	0.104	BD		
	25%	>500	0.006	BD		
	50%	>500	0.000	BD		
Note: Measurements Made with Yokogawa MY 40 Resistance Break Down Meter						

Despite the obvious issue with initial scribe resistance, the resultant Na diffusion data appears to proceed along a trend that is consistent with standard Na diffusion testing. Figure 32 shows raw data for 8 of the 10 applied scribes. We can see that there is a rapid decrease in the resistance of the scribe with time with all scribes effectively behaving like short circuits in a matter of hours. From a process perspective, this is obviously an unacceptable result. Abound solar reports that and acceptable scribe must exhibit little to no degradation in this test. It was previously mentioned that it is possible the 30 um scribes were too narrow and damaged by arcing due to the applied voltage. It is possible that damage to the scribe in this way could potentially result in anomalous Na diffusion rates. However, for this analysis we will assume that the exponential degradation is an indicator of the rate at which Na diffuses from the substrate into the film and that this rate is an indicator of the of the intrinsic resistance of the laser scribe to Na diffusion.

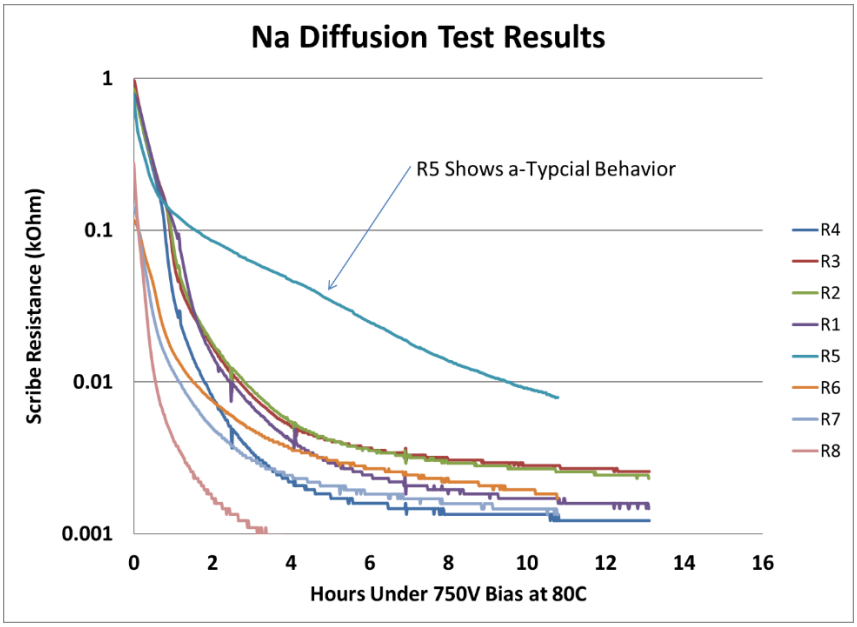

FIGURE 32: RAW NA DIFFUSION TEST DATA PROVIDED BY ABOUND SOLAR.

The curves of Figure 32 show an obvious exponential rate behavior. To analyze the data further each curve was normalized to its own beginning resistance value and fit to an exponential and the rate constant extracted. For a more intuitive sense of the degradation rate, the first 18 minutes of degradation was also fit to a line to extract the approximate linear degradation rate in kOhm per hour. The results of this analysis are shown below in Figure 33. The data thus far has been quite disappointing, however in the analysis of the rate coefficients we can see a very clear trend. Namely, as the laser scribe conditions become more aggressive, the scribes exhibit a faster degradation rate. For example, scribes R1 through R5 and R6 through R10 represent a progressive increase in the amount of material that the laser scribe removes (Figure 34). The laser scribe with the slowest degradation rate is R6 which clearly retains the thickest barrier layer and degradation rates increase with increasing removal of the barrier layers. It appears that at least there is some impedance of Na migration into the scribe by the remaining material at the bottom of the scribe.

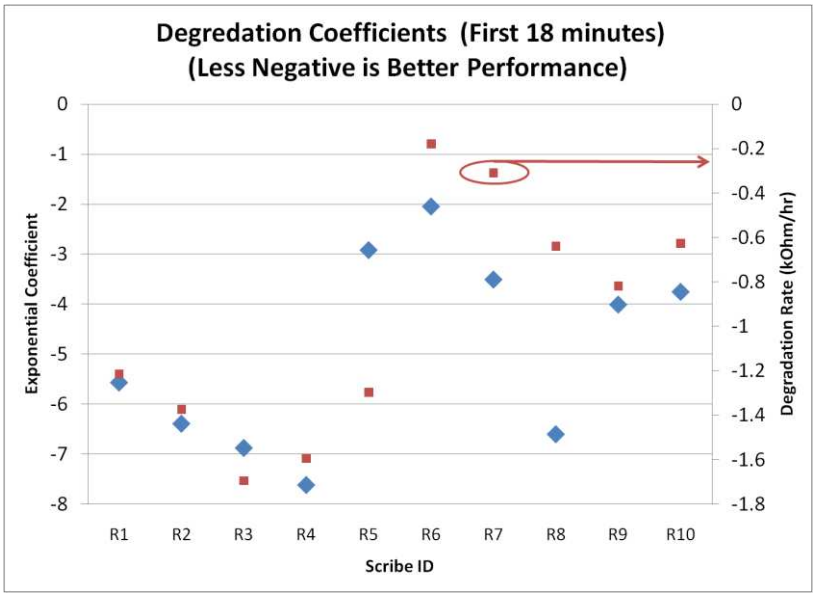

FIGURE 33: ANALYSIS OF DEGRADATION RATES IN THE FIRST 18 MINUTES OF THE NA DIFFUSION TEST. LEFT SCALE IS THE EXPONENTIAL RATE COEFFICIENT AND THE RIGHT SCALE THE SLOPE OF THE LINEAR APPROXIMATION TO THE EXPONENTIAL CURVE IN THE FIRST 18 MINUTES. (NA DIFFUSION TEST DATA GATHERED BY ABOUND SOLAR, DATA ANALYSIS PERFORMED BY MATT REKOW).

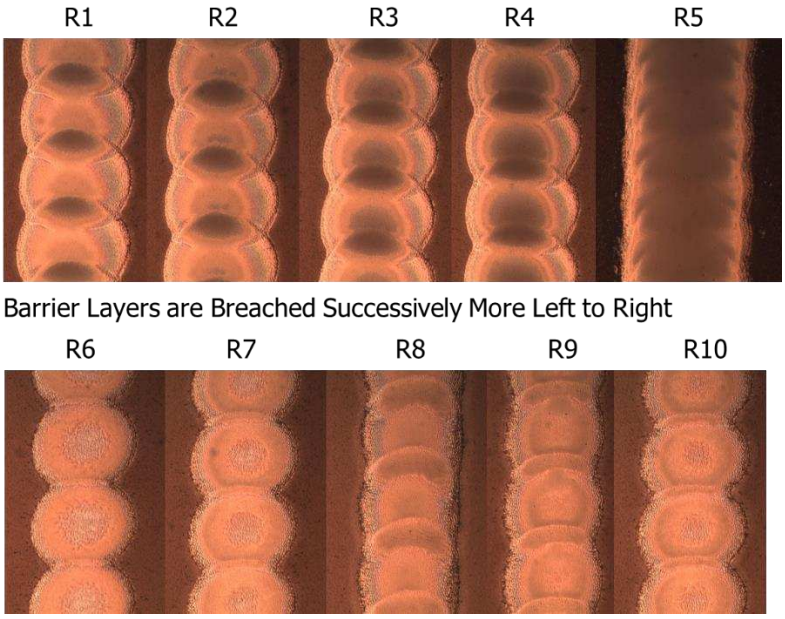

FIGURE 34: MORPHOLOGY OF LASER SCRIBES APPLIED TO NA DIFFUSION TEST SAMPLES. TOP ROW REPRESENTS A "SQUARE" PULSE OF INCREASE PULSE DURATION AND THE BOTTOM ROW REPRESENTS A CHAIR PULSE OF INCREASING "SEAT" DURATION.

Finally, we performed EDX analysis of the along sample laser scribe lines with similar scribing parameters to those used in the Na diffusion tests (Figure 35). The results of these measurements appear to confirm that breaching the barriers layers does result the appearance of Na on the groove surface while preserving the barrier layers results in

a groove bottom that is relatively Na free. In principle, this is in qualitative agreement with the fact that the aggressive parameters exhibited faster degradation rates. It also confirms that the SiO_2/SnO_2 do in fact inhibit Na diffusion if left intact, however apparently, they are still too permeable at least under a 750 Volt bias.

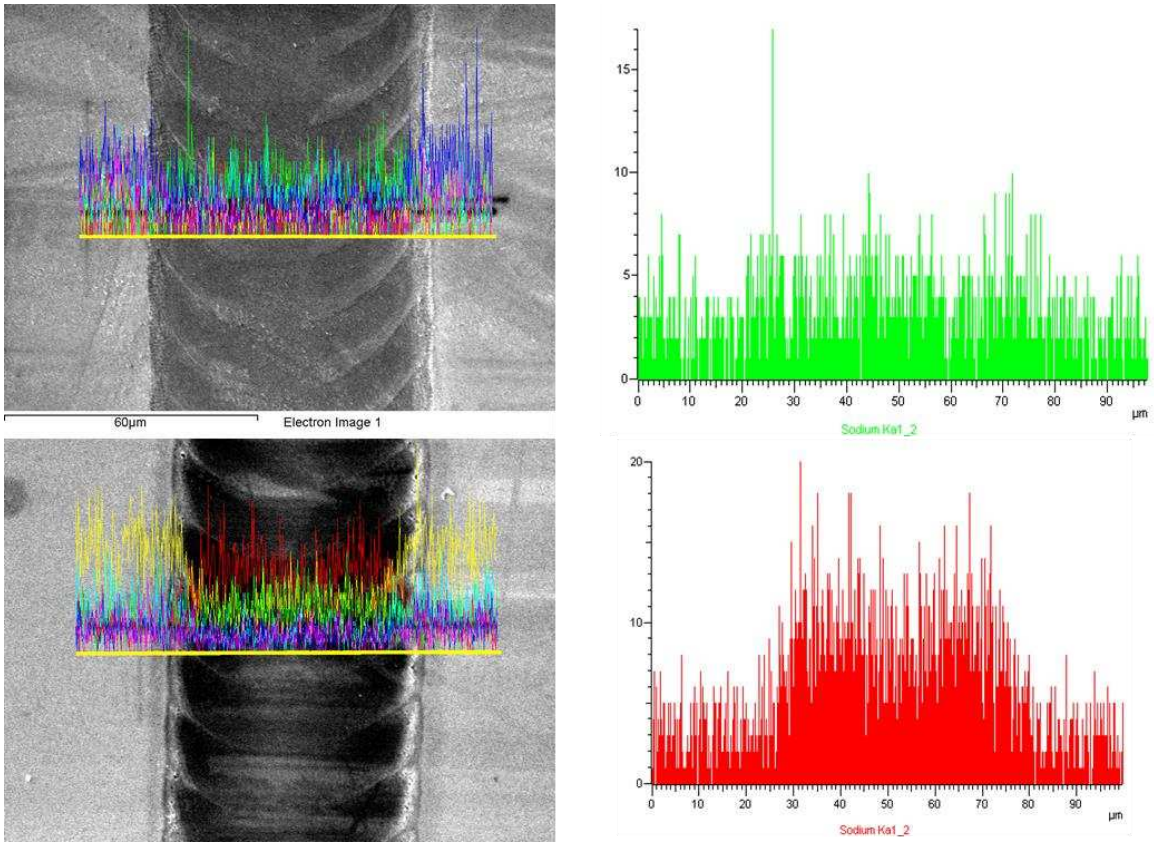

FIGURE 35: SEM/EDX ANALYSIS OF LASER SCRIBES. THE TOP FIGURES REPRESENT A SCRIBE LINE CONSISTENT WITH THE LESS AGGRESSIVE PARAMETERS USED IN SCRIBE R6 AND THE BOTTOM FIGURES REPRESENT A SCRIBE CONSISTENT WITH AGGRESSIVE PARAMETERS USED IN SCRIBE R5. THE PLOT AT RIGHT REPRESENTS THE RELATIVE ABUNDANCE OF NA ALONG A LINE CROSSING THE SCRIBE. (EDX ANALYSIS PERFORMED BY NRC LONDON, ONTARIO CANADA).

6.6 DISCUSSION

As mentioned the results of these tests were a disappointment and follow up tests to confirm the results were never performed due to the changing economic climate in the solar industry. There are questions regarding the methodology and geometry of the scribe lines that suggest it is possible this negative result is an artifact of test methodology. As a final observation, the Na diffusion test was designed to test an existing process in which a

relatively wide scribe is created, removing both CdS and CdTe and filling the resulting groove with an insulating material. This new process is fundamentally different in that CdS/CdTe fills the P1 groove and the P1 groove is relatively narrow. It is possible that the Na diffusion test as applied was not applicable to this structure and may not be giving relevant results. With these deficiencies recognize, normal scientific investigation would lead us to repeat the experiments in a more rigorous way. It is the authors hope that this work will find application in other areas or perhaps lead to improvements in CdTe solar panel manufacturing which as of this writing is the only thin film solar technology that remains competitive with low cost polycrystalline PV for industrial scale power generation.

7.0 SUMMARY AND CONCLUSION

In this work, we have also identified what could be viewed as a possible new class of laser ablation. Specifically, it could be accurately called photo-chemical laser etch. We propose a physical model for this ablation mechanism that involves optical interaction of laser light with surface defect states in the semiconductor, preferential surface absorption and heating, followed by chemical dissociation of SnO_2:F. This process proceeds monotonically from the surface inward and is only a function of the duration of the laser pulse. This allows precise and selective removal of the SnO_2:F while preserving underlying layers.

In this work we have shown that it is indeed possible to produce a laser scribe on TEC10 glass that removes only the SnO_2:F leaving the SiO_2 and the SnO_2 layers intact utilizing a very specific controlled laser pulse temporal profile. We also demonstrated that the resulting scribes had resistance values in the range of 100's of kOhm and the barrier layers did not appear to be physically breached. This is lower than is typically expected for the P1 laser scribe but sufficient to produce solar cells with negligible shunt losses. Preliminary testing gave disappointing results regarding the effectiveness of these remaining barrier layers in reducing sodium diffusion. However, upon closer examination of the test conditions and test results, it seems possible that the negative test results may be related to scribe width that was too narrow, resulting in electrical arcing. It may also be possible that the Na diffusion test protocol may not have been a valid test for the scenario where the semiconductor layers were not completely cut through. It would be reasonable to attempt to reproduce this test correcting the obvious mistakes in protocol.

In addition, we demonstrated how this process could be utilized to make diffractive, colorful markings in the SnO_2:F films. In addition, it is apparent that this process could be used to write electronic circuits in the transparent conductive films. For example, traces could be patterned on the circuit and resistors could be introduced by accurately thinning the trace.

In conclusion, this novel laser-material interaction phenomenon has potential to enable new processes in both solar and other fields. It is the author's strong opinion that the negative Na diffusion test result is artifact of the of the narrow scribe width chosen for these test, not an indicator of real Na diffusion. It is the author's hope that

eventually this work will be continued to confirm whether the alternate P1 scribe process could further simplify CdTe solar panel manufacturing and that other fields may also find application for this unique process.

WORKS CITED

1. **N. Romeo, A. Bosio, R. Tedeschi and V. Canevari.** Growth of polycrystalline CdS and CdTe thin layers for high efficiency thin film solar cells . *Materials Chemistry and Physics.* 2000, Vol. Volume 66, Issues 2-3.

2. **Sampath, W. S.** Private Communication. 2011.

3. *CdTe solar cells with open-circuit voltage breaking the 1 V barrier.* **al, J.M. Burst et.** 16015, s.l. : Nature Energy , 2016, Vol. 1.

4. **Britannica, The Editors of Encyclopædia.** soda-lime glass. *Encyclopædia Britannica.* [Online] Encyclopædia Britannica, inc., August 28, 2008. [Cited: Feb 18, 2017.] https://www.britannica.com/technology/soda-lime-glass.

5. **Wager, John F., Keszler, Douglas A., Presley, Rick E.** *Transparent Electronics.* s.l. : Springer, 2008. ISBN 978-0-387-72342-6.

6. **LIA.** *LIA Handbook of Laser Materials Processing.* Orlando : Magnolia Publishing Inc, 2001. 0-941463-02-8.

7. **K. VON ROTTKAY, M. RUBIN.** Optical Indeces of Pyrolytic Tin-oxide glass. *Mater. Res. Soc. Symp.* 1996.

8. *Application of a Pulse Programmable Fiber Laser to a Broad Range of Micro-Processing Applications.* **Rekow, M, et al.** Anaheim : LIA, 2010.

9. *Modification of dielectric surfaces with ultra-short laser pulses.* **Costache, Florenta, Matthias Henyk, and Jürgen Reif.** 2002, Applied surface science, Vol. 186.1, pp. 352-357.

10. *Observations of higher-order laser-induced surface ripples on ⟨111⟩ germanium.* **Fauchet, P. M..Siegman, A. E.** 2, s.l. : Springer Berlin / Heidelberg, 11 1, 1983, Applied Physics A: Materials Science & Processing, Vol. 33. 0947-8396.

11. *Surface structures on crystalline silicon irradiated by 10 ps laser pulses at 694.3 nm.* **Lee, T. D., Lee, H. W.,Kim, J. K.,Park, C. O.** s.l. : Springer Berlin / Heidelberg, 1989, Applied Physics A: Materials Science & Processing. 10.1007/BF00619721.

12. **L. V. Gurvich, I. V. Veyts, C. B. Alcock.** *Thermodynamic Properties of Individual Substances: Part 1, Volume 2Elements C, Si, Ge, Sn, Pb and Their Compounds.* Moscow : Hemisphere Publishing Corporation, 1979. ISBN 0-89116-533-9.

13. **Mol, Antonius Maria Bernardus van.** Chemical Vapour Deposition. *Thesis.* s.l. : Technische Universiteit Eindhoven, 2003.

14. *Photoreflectance Probing of Below Gap States in Gan/Algan High Electron Mobility Transitor Structures.* **D. K. Gaskilla, O. J. Glembockia, B. Peresa, R. Henrya, D. Koleskea and A. Wickenden.** s.l. : MRS, 2002.

15. *Infrared studies on SnO2 and Pd/SnO2.* **D. Amalric-Popescu, F. Bozon-Verduraz.** 2001, Catalysis Today, Vol. 70, pp. 139–154.

16. *Thermal dissociation of compressed ZnO and SnO2 powders in a moving-front solar thermochemical reactor.* **Marc Chambon, Stéphane Abanades*, Gilles Flamant.** 8, s.l. : AIChE Journal, 2010, Vol. 57. DOI: 10.1002/aic.12432.

17. *Understanding and Enabling Laser Processing of Solar Materials through Temporal Pulse Control.* **M. Rekow, T. Panarelloa, N. Fallettoa. M. Guevremonta,.** San Diego : SPIE, 2012.

18. *Selective Removal of TCO Stack Layers for CdTe P1 Process with a Tailored Pulse Laser.* **M. Rekow, R. Murison, C. Dinkel, T. Panarello, S. Nikumb, W. S. Sampath.** Seattle : IEEE PVSC Proceedings, 2011.

19. **Chen, J.** *Spectroscopic Ellipsometry Studies of II-VI Semiconductor Materials and Solar Cells.* Toledo : The University of Toledo, 2010.

21. **Kozlowski, Mark.** *Fabrication of Low Defectivity Electrochromic Devices. 0243427* USA, Sept 30, 2010. Applications.

22. **Murison, R, et al.** *7742511* 2008.